Hydrogeomorphology of the hyporheic zone: Stream solute and fine particle interactions with a dynamic streambed

J. W. Harvey,[1] J. D. Drummond,[2] R. L. Martin,[3] L. E. McPhillips,[1] A. I. Packman,[2] D. J. Jerolmack,[3] S. H. Stonedahl,[2] A. F. Aubeneau,[2] A. H. Sawyer,[4] L. G. Larsen,[1] and C. R. Tobias[5]

Received 31 March 2012; revised 15 August 2012; accepted 24 August 2012; published 9 October 2012.

[1] Hyporheic flow in streams has typically been studied separately from geomorphic processes. We investigated interactions between bed mobility and dynamic hyporheic storage of solutes and fine particles in a sand-bed stream before, during, and after a flood. A conservatively transported solute tracer (bromide) and a fine particles tracer (5 μm latex particles), a surrogate for fine particulate organic matter, were co-injected during base flow. The tracers were differentially stored, with fine particles penetrating more shallowly in hyporheic flow and retained more efficiently due to the high rate of particle filtration in bed sediment compared to solute. Tracer injections lasted 3.5 h after which we released a small flood from an upstream dam one hour later. Due to shallower storage in the bed, fine particles were rapidly entrained during the rising limb of the flood hydrograph. Rather than being flushed by the flood, we observed that solutes were stored longer due to expansion of hyporheic flow paths beneath the temporarily enlarged bedforms. Three important timescales determined the fate of solutes and fine particles: (1) flood duration, (2) relaxation time of flood-enlarged bedforms back to base flow dimensions, and (3) resulting adjustments and lag times of hyporheic flow. Recurrent transitions between these timescales explain why we observed a peak accumulation of natural particulate organic matter between 2 and 4 cm deep in the bed, i.e., below the scour layer of mobile bedforms but above the maximum depth of particle filtration in hyporheic flow paths. Thus, physical interactions between bed mobility and hyporheic transport influence how organic matter is stored in the bed and how long it is retained, which affects decomposition rate and metabolism of this southeastern Coastal Plain stream. In summary we found that dynamic interactions between hyporheic flow, bed mobility, and flow variation had strong but differential influences on base flow retention and flood mobilization of solutes and fine particulates. These hydrogeomorphic relationships have implications for microbial respiration of organic matter, carbon and nutrient cycling, and fate of contaminants in streams.

Citation: Harvey, J. W., et al. (2012), Hydrogeomorphology of the hyporheic zone: Stream solute and fine particle interactions with a dynamic streambed, *J. Geophys. Res.*, *117*, G00N11, doi:10.1029/2012JG002043.

1. Introduction

[2] Transport of solutes and suspended materials through streams is never a steady process. Transport and storage processes are constantly re-adjusting to variations in streamflow and corresponding modifications of geomorphic roughness features. For example, hyporheic flow beneath small bedforms is strongly influenced by current-driven forces on the streambed that are affected both by changes in streamflow velocity [*Boano et al.*, 2007] and by adjustments in the size and shape of bedforms [*Thibodeaux and Boyle*, 1987]. Hyporheic flow beneath larger geomorphic features such as riffles and bars is also highly responsive to flood-driven expansion of the stream's planform and changes in bar submergence [*Wondzell and Swanson*, 1996]. Whereas bars, riffles, banks, and floodplains are shaped by the largest and most infrequent floods, smaller features such as sand ripples actively migrate during relatively minor variations in flow [*Nittrouer et al.*, 2008; *Carling et al.*, 2000; *Dade and Friend*, 1998; *Nelson and Smith*, 1989].

[3] The effect of fluctuating stream discharge on hyporheic flow has been studied in flumes [*Elliott and Brooks*, 1997] and investigated numerically [*Boano et al.*, 2007; *Karwan*

[1]National Research Program, U.S. Geological Survey, Reston, Virginia, USA.
[2]Department of Civil and Environmental Engineering, Northwestern University, Evanston, Illinois, USA.
[3]Department of Earth and Environmental Science, University of Pennsylvania, Philadelphia, Pennsylvania, USA.
[4]Geological Sciences, University of Delaware, Newark, Delaware, USA.
[5]Marine Sciences, University of Connecticut, Groton, Connecticut, USA.

Corresponding author: J. W. Harvey, National Research Program, U.S. Geological Survey, 430 National Center, Reston, VA 20192, USA. (jwharvey@usgs.gov)

0148-0227/12/2012JG002043

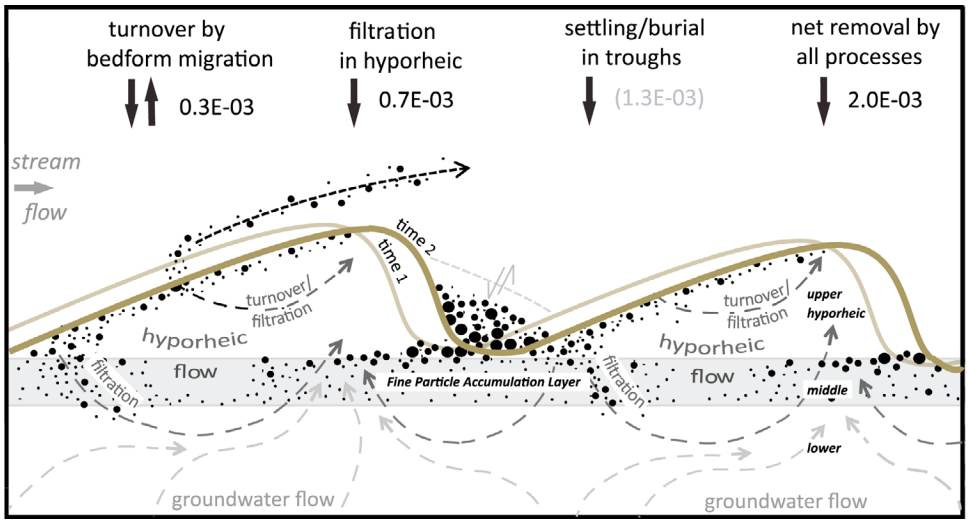

Figure 1. Conceptual model of solute and fine particulate transport in a sand-bed stream. Mechanisms of storage common to both include conservative storage-exchange associated with turnover of migrating bedforms and conservative transport through hyporheic flow paths (not shown). Removal of fine particulates occurs by flocculation and settling to the streambed, filtration in hyporheic flow paths, and return to streamflow by entrainment due to storm-induced growth of bedforms. Summarized fluxes are uptake velocities in cm s^{-1}, with settling/burial in troughs estimated by the difference between net removal and removal by hyporheic filtration. This figure shows that fluxes occur at similar timescales but are active at different depths in the subsurface, which results in the accumulation of fine particulates in a layer beneath bedforms. Floods differentially mobilize solutes and fine particles, entraining the more shallowly deposited fine particles while driving solutes into deeper hyporheic flow paths beneath larger flood-created bedforms (see text).

and Saiers, 2012]. Temporally varying streamflow has been shown to strongly influence hyporheic flow both seasonally [*Harvey et al.*, 1996] and on diel timscales [*Gerecht et al.*, 2011]. Many researchers have emphasized links between dynamic hyporheic flow and stream ecology. For example, hydraulic disturbance of algal, periphyton, and microbial biofilm communities is increasingly being studied to understand how stream ecosystems recover from floods [*Valett et al.*, 1994; *Battin et al.*, 2003; *Arnon et al.*, 2010; *O'Connor et al.*, 2012]. Attention is increasingly being given to understanding how these factors affect dissolved oxygen uptake and accompanying biogeochemical reactions in the hyporheic zone [*O'Connor and Hondzo*, 2008], transport of nutrients associated with fine particulates [*Harvey et al.*, 2011], metal cycling [*Brigham et al.*, 2009] and transport and fate of pathogenic bacteria [*Searcy et al.*, 2006]. These topics also are integral to understanding organic matter cycling and metabolism [*Paul and Hall*, 2002; *Minshall et al.*, 2000; *Battin et al.*, 2008; *Newbold et al.*, 2005; *Webster et al.*, 1987] and predicting how streams will respond to changing flood regimes due to land-use and climate change [*Mulholland et al.*, 2008; *Bukaveckas*, 2007; *O'Connor et al.*, 2010]. Rarely, however, have the combined effects of flow and geomorphic change on hyporheic flow been investigated.

1.1. Processes Linking Bedform Mobility, Dynamic Hyporheic Flow, and Fate of Solutes and Fine Particulates

[4] Downstream transport of solutes and fine particulates is delayed by exchange between the actively flowing main channel and more slowly moving waters located on channel sides, bottoms of pools, recirculating areas behind various roughness features, and hyporheic flow paths through the streambed. Exchange with these "storage zones" increases the residence time and contact area of solutes and fine particulate organic matter (FPOM) with biologically active areas on and within the streambed [*Lautz and Fanelli*, 2008; *Harvey and Fuller*, 1998]. Compared with solutes, fine particulates are subject to additional mechanisms, such as gravitational settling to the bed [*Dietrich*, 1982; *Tipping et al.*, 1993], flocculation [*Larsen et al.*, 2009], deposition on stems of aquatic vegetation [*Saiers et al.*, 2003; *Palmer et al.*, 2004], aggregation with organic matter [*Einstein and Krone*, 1962; *Thomas et al.*, 2001], and subsurface filtration, which is a combination of settling or straining within pores spaces and attachment by weak bonding to mineral or organic surfaces [*Packman et al.*, 2000; *Karwan and Saiers*, 2009]. In highly turbulent streams where turbulent transfer may dominate vertical movement of fines in the water column, settling still may play a role in the laminar sub-layer just above the bed, and also in storage zones near channel sides or in subsurface hyporheic flow paths. The combined effects of turbulent transfer, settling, and filtration in hyporheic flow paths can result in accumulation of fine particulates on and within the streambed [*Hünken and Mutz*, 2007; *Packman et al.*, 2000]. Mobilization of fine particulates from the bed is generally more difficult to predict because often thresholds in shear stress must be surpassed to initiate motion [*Harvey et al.*, 2011]. Frequently the streambed bed itself must be disturbed by scour or migration of bedforms in order to entrain fine particulates (Figure 1).

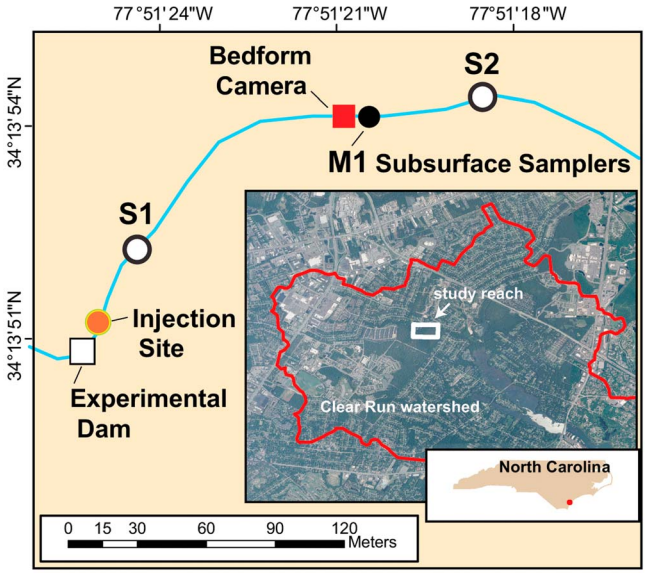

Figure 2. Location of streamflow manipulation and injection of solute and fine particulates tracers in Clear Run, a sand-bed stream located on the Atlantic coastal plain near the city of Wilmington, NC. The inset photograph shows the location within the rapidly urbanizing 9.4 mi^2 Bradley Creek watershed in southeastern North Carolina. Transport processes were investigated over a distance of 221 m between the injection site and site S2. The sub-reach between the injection and S1 was a 47-m mixing reach followed by a 174-m experimental sub-reach between S1 and S2. Also shown is the location of time-lapse photography to image bedform migration (CAMERA) and location of in situ hyporheic sampling of tracers in the streambed (M1).

[5] Changing flow velocity and bedform growth and decay during floods should adjust current-driven hyporheic flow in the shallow streambed. In theory, as shear stress near the bed increases, the hyporheic flux will increase with the square of velocity and decrease proportionally with bedform wavelength [*Elliott and Brooks*, 1997]. The depth of hyporheic flow also will increase beneath larger bedforms [*Elliott and Brooks*, 1997; *Cardenas and Wilson*, 2007]. Average residence time of hyporheic flow therefore adjusts during floods based on greater current-driven forces driving flow through longer and deeper flow paths. Migration of bedforms increases surface-subsurface exchange of solutes and fine particulates [*Packman and Brooks*, 2001; *Packman and MacKay*, 2003] and reduce clogging of the streambed interface with fines [*Rehg et al.*, 2005]. Simultaneous geomorphic and hydrologic adjustments could be further complicated by relative timescales of hyporheic flux and growth and decay of flood-created bedforms. These dynamic interactions between transport and geomorphic processes (Figure 1) have rarely been addressed in the field.

[6] Our study had the purpose to evaluate temporally varying hyporheic and geomorphic dynamics in a sand-bed stream, with a goal to understand these effects on solute and fine particulate organic matter transport. For this study fine particles had a diameter less than approximately 5% of the bed grain diameter (i.e., 20 μm or less in a medium sand streambed) which is fine enough to penetrate an unarmored streambed. Our study is the first we are aware of to quantify solute and fine particulate transport processes in situ during a flood and to outline the principal competing factors and timescales involved. In addition to characterizing transport dynamics at the reach scale, we directly measured in situ transport and filtration of fines in hyporheic flow paths as well as the exchange by entrapment and release of solutes and fines with migrating bedforms. We directly quantified transport and retention processes both at the reach-scale and the scale of the principal geomorphic unit, i.e., dune-shaped bedforms and associated hyporheic flow paths beneath them. Conservatively transported solutes penetrated the bed more deeply than fine particulates that filtered between sand grains, which created differential responses to a flood. To aid in interpreting the results of our field experiment we refer several times to the recently developed model by R. L. Martin and D. J. Jerolmack (Origin of hysteresis in bedform response to unsteady flows, submitted to *Water Resources Research*, 2012). Although fines were easily entrained by the shallow physical disturbance associated with formation and migration of bedforms, solutes were stored longer during a flood due to the deepening of hyporheic flow paths beneath flood-formed bedforms.

2. Research Site

[7] Clear Run is a shallow, fast-flowing, sand-bed stream within the Bradley Creek watershed on the Atlantic coastal plain of eastern North Carolina near the city of Wilmington, NC (Figure 2). The watershed is moderately to heavily urbanized, averaging 23% impervious surface within its 9.4 sq. miles. The study reach was located in a wooded and sparsely developed part of the UNC-Wilmington college campus, which was selected due to its controlled access and the ability to construct a small experimental dam. However, Clear Run originates just 1 mile upstream within a major

Figure 3. (a) Solute and fluorescent particulate tracers were injected into Clear Run for 3.5 h during a time period of steady base flow. (b) One hour after the injections ceased a small flood was created by releasing water through the dam. Before and after the flood, (c) time-lapse photo imaging of bedform migration was conducted using a tripod mounted camera that had been programmed to shoot on 30 s intervals as well as (d) in situ sampling of solute and fine particulate tracer breakthrough at shallow depths in the streambed using the USGS MINIPOINT sampler.

commercial corridor, making the stream flashy in response to storms. Within the study reach Clear Run is a second-order stream with a 3-m wide incised channel bounded by stable 1-m tall banks and flanked by a forested riparian floodplain that is approximately 75-m wide. Typical streamflow is approximately 60 L/s with frequent higher flows caused by winter cold fronts, summer thunderstorms, and occasional extratropical storms. The streambed is composed of well sorted medium sand shaped by the flow into dune-shaped bedforms that migrate steadily in the downstream direction. The planform of the stream is almost straight with very gentle meanders, without pools or riffles, and with very few features such as embayments at channel sides or logs in the stream that create large storage zones. The most obvious storage zones are in surface and subsurface zones associated with the migrating bedforms. In addition to hyporheic flow beneath bedforms, flow recirculates in the troughs between bedforms. In the troughs we observed the collection of coarse particulate organic matter (CPOM) that shuttled downstream as bedforms migrated. Small pockets of CPOM were also buried in the streambed although observations were sparse as the streambed is dominantly medium sand.

3. Methods

3.1. Overview of Field Experiment

[8] In the weeks prior to the experiment a small dam was constructed by building a lumber frame and anchoring it in trenches excavated into the stream banks with cinder blocks attached with galvanized hardware (Figure 3a). The frame supported removable 2″ × 6″ wood panels that spanned the channel. A metal sheet wall was driven beneath the bottom stop log to a depth of several feet into the sand bed in order to lessen underflow. On the day prior to the tracer experiment the dam was closed with stop logs. After several hours, the dam reservoir filled and the stream flowed over the spillway to reestablish steady downstream flow. On the following day (18 September 2009 at 12 P.M.), with the dam still full and overflowing, we began a 3.5 h steady co-injection of bromide and fluorescent latex particles into the mixing zone in front of the dam. Surface water sampling for all tracers started one half hour before the first injections began and continued throughout the afternoon and evening.

[9] The experimental flood was initiated 4.5 h after the tracer injections started (i.e., 1 h after tracer injections were shut off). The flood was started by removing the dam's stop logs several at a time over a period of a few minutes (Figure 3b). A second conservative solute tracer (chloride) was injected with the flood water in order to estimate the flood discharge and velocity, and supported by supplemental velocity gaging measurements at a downstream location. Before, during, and after the flood we observed bedform migration using an overhead camera mounted above the stream at a site 183 m downstream of the injection (Figures 2 and 3c). At a short distance downstream of the camera location we sampled tracer concentrations at multiple depths within hyporheic flow paths and in underlying groundwater (Figure 3d). Changes in surface water level were measured over the course of the experiment at a location in the central channel just downstream of the camera and hyporheic sampler. Measurements were made with a recording pressure transducer in a (1.5″ nominal) PVC tube with a slotted screen

driven vertically into the sandy substrate. The pressure transducers were periodically calibrated by manual tape-downs from a point of fixed elevation to the water surface.

3.2. Solute and Fine Particulate Tracer Injections

[10] The solute tracer (bromide) was injected at a rate of 102 ml/min from a reservoir containing 59 kg of potassium bromide (KBr) mixed in 36 L of deionized water. The fine particulate tracer was prepared in a separate reservoir by adding 1.0 kg of dry fluorescent paint powder (DayGlo Fluorescent AX Pigments-Aurora Pink) to a 76 L surfactant-stream water mixture (5 g L^{-1} of Alfa Aesar sodium hexametaphosphate) in order to disperse and wet the fluorescent particles, which are slightly hydrophobic. The tracer particles range in size from 1 to 10 μm in diameter, averaging approximately 5 μm, and have a density of 1.36 g cm^{-3} which is similar to the typical density of fine particulate organic matter 1.3 g cm^{-3} [*Cushing et al.*, 1993]. The AX particles in aqueous suspension with surfactant are moderately stable, as indicated by a zeta potential of −29 mV. To remain stable and prevent flocculation, the injection suspension was continuously mixed with a paint stirrer attached to a battery-powered drill mounted above the reservoir.

[11] The bromide and fine particulate tracer injections both began at 12:00 P.M. and ended at 3:30 P.M., one hour before the flood started. The chloride tracer injection began simultaneously with the flood at a rate of 6,902 ml/minute into flood flow over the dam from a reservoir containing 88 kg of sodium chloride mixed in 95 L of deionized water. After the flood discharge had peaked (approximately 11 min) the rate of injection of the chloride tracer was cut approximately in half to 3,313 ml/min in order to prevent chloride concentrations from increasing to excessive levels during base flow.

3.3. Bedform Dynamics

[12] Bedform dynamics were characterized by time-lapse photographic imaging of the streambed that revealed size and migration patterns of bedforms before, during, and after the experimental flood. A Nikon D5000 camera was attached and leveled at a point 2.5 m above the stream on a boom extending from a tripod set up on the stream bank. Time-lapse images of bedform migration were captured every 30 s during two time periods: one at steady base flow conditions, and the other during the dam-release flood wave. The field of view covered an area of 190 cm in the longitudinal direction and 106 cm in the transverse direction with a pixel resolution of 0.66 mm. Bedform crestlines were detected on photos by shading differences in coloration of sand. Bedform troughs were detected by the presence of coarse particulate organic matter trapped within them that appears on photos as dark streaks.

[13] Bedform wavelengths were estimated by measuring longitudinal distances between bedform troughs in selected images of the bed. We manually traced out these troughlines of bedforms in an image, then we measured trough-trough distances along horizontal image transects to determine the distribution of bedform wavelengths. Given the sparse number of bedforms present in the imaging window during the flood, we could not fit a statistical distribution to bedform wavelengths for the flood. The rate of bedform migration at base flow and during the flood was measured by tracing the propagation of troughlines of individual bedforms on successive images and calculating an average migration rate for each bedform from the slope of a best fit line of troughline position versus time. Migration distances of 10 randomly selected bedforms were determined during base flow and averaged using this method. Five randomly selected bedforms were traced during the flood peak.

[14] Average bedform height was determined from measurements of the length of downstream slipfaces on bedforms on photographic images by estimating the distance between bedform crestlines and troughs. To calculate bedform height it was assumed that lee slipfaces of bedforms adjust to the angle of repose for sand, approximately 30 degrees, which translates to a height of the ripple equal to half of the length of the slipface.

3.4. Subsurface Sampling of Solute and Fine Particulate Tracers

[15] Tracers were sampled in situ at multiple depths below the streambed using USGS MINIPOINT samplers with multichannel pumps. Design specifications and integrity testing of the USGS MINIPOINT sampler and quantitative analysis approaches for tracer studies are previously documented by *Duff et al.* [1998] and *Harvey and Fuller* [1998], respectively. Hyporheic sampling was conducted beneath sandy bedforms near the channel center at a location approximately 5 m downstream of the location of bedform photo-imaging (Figure 3d). Small-volume (10-ml) samples were pumped simultaneously at low rates (1.5 ml/minute) from seven 1/8-inch (nominal outside diameter) stainless-steel sampling tubes. One surface water point and ten subsurface points were sampled at depths of −2.5, 1.5, 3, 5, 8, 12, 20, 30, 40, 60 and 75 cm. The depths refer to the vertical distance beneath the average elevation of the streambed surface (i.e., midpoint of bedform height). Pumping at low rates during and after the tracer experiment produced a time series of approximately twenty-four water samples from each sample point. All hyporheic water samples were pumped through Masterflex size 13 tygon tubing, which has very low gas permeability. Short lengths of more durable and flexible Norprene^{tm} tubing were used in the multihead pumps. Samples for solute analyses were pumped directly through sealed in-line 25 mm 0.2 μm pore size, Pall polyethersulfone filters and then directly into 20-ml LDPE plastic scintillation vials with polyseal^{tm} caps. Prior to collecting fine particulate tracer samples, filters were removed and lines flushed before filling vials. Similar tracer sampling was also conducted in the stream bank.

[16] Although the MINIPOINT samplers worked very well to observe tracer movement into hyporheic flow paths beneath bedforms during base flow, they were not effective during the flood. This was because of varying amounts of scour around samplers created by capture of wet leaves on sampling tubes during the flood. Approximately 10 cm from the sampling tubes there was a maximum of 2 cm of scour, which we considered significant enough to discount the subsurface tracer measurements during that period. Fortunately the in situ samplers installed in the stream bank were not affected by flood scour, which allowed us to rule out bank storage as an important contributor to tracer storage dynamics.

3.5. Physical Characteristics of Streambed Sediment

[17] Streambed sediment was cored to measure the grain size distribution, porosity and organic carbon content in the top 6 cm. In addition, grab samples were taken from the streambed surface to characterize grain size and variability in the migrating bedforms. Coring was accomplished by pushing 10-cm long clear polycarbonate cylinders (nominally 0.048 m internal diameter by 0.00159 m wall) that had been sharpened at one end into the streambed. Stream water was added to fill any remaining headspace and cores were capped with butyl rubber stoppers and removed from the streambed. After removal the cores were immediately extruded, sectioned into 1-cm increments relative to the average height of the streambed surface, bagged, and then returned to the laboratory where they were dried to a constant weight in a 60°C oven. Porosity was determined for each core increment assuming a grain density of 2.65 g cm^{-3}. The grain size distribution was determined by dry sieving samples through 1000, 500, 250, 125, and 60 μm diameter sieves on a Gilson Model SS-3 shaker and reweighing each size fraction.

[18] Streambed sediment grab samples of approximately 2 cm in depth were collected from the central stream at 11 sites spaced approximately 20 m apart along the experimental reach. At each location, one sample was collected from a bedform trough and one sample from a bedform crest. In the laboratory the samples were dried to constant weight in a 60°C oven and grain size distribution was measured by particle imaging techniques using a Retsch Camsizer. Several intact cores were obtained from the vicinity of the site of bedform photo-imaging and subsurface tracer sampling.

[19] Organic carbon was determined in streambed sediment from core samples after sieving was completed. The sieved core samples were composited into $\geq$250 μm and $<$250 μm fractions. Three replicates of each fraction were sub-sampled for elemental CHN analysis. Analyses were performed on a Thermo Scientific/CE Elantech CHN analyzer and with use of a 6-point calibration curve based on readings of an atropine standard. All samples were run in triplicate and reported in units of carbon as a percentage of total sample weight.

[20] Streambed sediment hydraulic conductivity, K, was measured in the field by performing approximately 21 field permeameter tests by inserting 0.048 m-diameter clear polycarbonate cylinders into streambed sediment to a depth of 0.1 m. A constant head test was conducted by pumping stream water continuously into the cylinders and monitoring the head until it stabilized [*Reynolds et al.*, 2002; *Landon et al.*, 2001].

3.6. Laboratory Analysis of Tracer Samples

[21] Tracer samples were analyzed in the laboratory over a period of several weeks following the completion of the tracer experiment. Bromide and chloride tracers were analyzed by ion chromatography (Dionex DX-120) with a Dionex AS-14 analytical column, AG-14 guard column, conductivity detector, 50 μl sample loop, and 3.4 mM sodium carbonate/1 mM sodium bicarbonate eluent. Our system has detection limits of 0.015 mg/L and 0.1 mg/L for bromide and chloride respectively, which easily allowed tracer concentrations to be distinguished from Clear Run background concentrations of bromide equal to 0.05 mg/L and 0.18 mg/L in surface water and deeper subsurface water respectively, and a background concentration of chloride equal to 12 mg/L.

[22] The fine particulate tracer was analyzed on a Becton Dickinson LSR II (San Jose, CA) equipped with FACSDiva 6.0 software and 488, 635 and 405 nm lasers. The emission filters used for the particles were 525/50 (Alexa Fluor 430) and 585/42 (PE) and final analysis was completed using FlowJo version 8.8.6 (Tree Star, Inc.). Forward scatter, side scatter, and fluorescent parameters were displayed in a log scale to include the range of size and fluorescence of the fluorescent pigment particles. Flow Check YG 6 μm Microspheres (Polysciences, Inc.) were added to each sample and used as a reference population for the direct determination of the sample volume analyzed by the flow cytometer.

3.7. Tracer Modeling Analysis

[23] The standard assumptions for modeling stream tracer experiments were applied to our experiments, including steady flow prior to the flood, complete tracer mixing in the main channel, along with others thoroughly documented in reviews such as *Harvey and Wagner* [2000]. There were several new aspects of this work. First we injected both solutes and fine particulates to load up storage zones at base flow and then followed with an experimental flood to examine tracer flushing effects. Second we measured tracer dynamics at multiple scales, i.e., at the stream reach scale of hundreds of meters and simultaneously at the geomorphic unit scale in samples collected in situ beneath sandy bedforms. Third we used a transport model with multiple storage zones that could potentially represent dynamics of storage in specific geomorphic units [see, e.g., *Briggs et al.*, 2009; *Harvey et al.*, 2005]. The reach scale measurements characterized the dominant spatial and temporal scales of storage without explicitly separating distinct types of storage. The in situ measurements, on the other hand, quantified storage associated with specific geomorphic features but, due to limited sampling, might not provide statistically valid estimates of whole-stream behavior. Therefore, by comparing transport and storage metrics across spatial scales we assessed the importance of hyporheic exchange beneath bedforms and estimated the cumulative effects on transport and fate of solutes and fine particulates in the stream as a whole.

3.7.1. Stream Discharge Analysis and Tracer Mass Balance

[24] Prior to modeling with OTIS-2stor, mass balance calculations were made using tracer measurements before and after the flood arrived. Streamflow discharge (Q) was estimated using the bromide tracer during base flow and the chloride tracer during the flood. Stream discharge was computed by dilution gaging estimation based on measured injection pump rates, measured injectate concentrations, and in-stream measurements of tracer concentration at the two in-stream sampling sites. Those estimates were compared with directly measured stream discharges made over the course of the experiment using a Sontek Flowtracker. The resulting discharge estimates were used to compute solute and fine particulate tracer mass balances before and after the flood. The mass balance integration was performed on 30 s increments by multiplying the measured streamflow

discharge by the measured in-stream concentration of solute or fine particulate tracers during pre-flood and post-flood time periods. Solute and fine particle tracer mass balances were determined by comparing total injected mass with integrated mass fluxes measured at the downstream end of the experimental reach. The tracer mass balances provided an overall assessment of the fate of tracers and revealed the relative importance of temporary storage-exchange versus longer term removal of tracers before and after the flood.

3.7.2. Reach-Scale Simulations

[25] The OTIS-2stor model is an extended version [*Choi et al.*, 2000] of the solute and fine particulate transport model of *Runkel* [1998] including both a faster and more slowly exchanging storage zone. Using two storage zones instead of one typically improves the model by simulating the broader range of storage timescales that have been observed in the field [e.g., *Neilson et al.*, 2010; *Briggs et al.*, 2009; *Choi et al.*, 2000] and that have been demonstrated theoretically [e.g., *Cardenas*, 2008]. As in all such experiments the longest storage timescales (in this case beyond the timescale of the more slowly exchanging storage zone) will be ignored, but such storage is probably not observable by any type of modeling given the inherent limitations set by injection time, travel time through the experimental reach, and uncertainty in the background tracer concentration [*Harvey and Wagner*, 2000].

[26] OTIS-2stor was used to estimate the reach-averaged characteristics of transport including advection and dispersion, groundwater inflow, solute and fine particulate exchange with storage zones, and the rate of removal of fine particulates. The governing equations of the OTIS-2stor model are

$$\frac{\partial C}{\partial t} = -\frac{Q}{A}\frac{\partial C}{\partial x} + \frac{1}{A}\frac{\partial}{\partial x}\left(AD_L\frac{\partial C}{\partial x}\right) + \frac{{q_L}^{in}}{A}(C_L - C) + \alpha_1(C_{S1} - C) + \alpha_2(C_{S2} - C) + \lambda_{Sed}, \quad (1)$$

$$\frac{dC_{S1}}{dt} = \alpha_1\frac{A}{A_{S1}}(C - C_{S1}) + \lambda_{S1,sed} \quad (2)$$

$$\frac{dC_{S2}}{dt} = \alpha_2\frac{A}{A_{S2}}(C - C_{S2}) + \lambda_{S2,sed} \quad (3)$$

where

C main channel concentration [mg l^{-1}]
Q volumetric flow rate [m^3 s^{-1}]
A main flow zone cross-sectional area [m^2]
D_L longitudinal dispersion coefficient [m^2 s^{-1}]
q_L^{in}, q_L^{out} lateral inflow and outflow rate [m^3 s^{-1} m^{-1}]
C_L lateral inflow concentration [mg l^{-1}]
α_1, α_2 storage zone 1 and 2 exchange coefficients [s^{-1}]
C_{S1}, C_{S2} storage zone 1 and 2 concentration [mg l^{-1}]
A_{S1}, A_{S2} storage zone 1 and 2 cross-sectional area [m^2]
λ_{sed} first-order deposition coefficient for fine particulates in stream [s^{-1}]
$\lambda_{S1,sed}$, $\lambda_{S2,sed}$ first-order deposition coefficient for fine particulates in storage zones [s^{-1}]
t time [s]
x distance [m].

[27] Streamflow discharge estimates from the previously described mass balance analysis were used, and groundwater discharge (q_L^{in}) was estimated by differencing streamflow estimates at several locations along the reach. The other transport parameters were estimated by inverse modeling using an extended version of the nonlinear least squares optimization procedure described in the documentation of OTIS [*Runkel*, 1998] and elaborated in *Harvey et al.* [2005]. The inversely estimated parameters included A, the average area of the main channel, D_L, the longitudinal dispersion parameter, which characterizes relatively fast mixing processes that achieve equilibrium in a given transport distance, and rate coefficients and cross-sectional areas (α_1, A_{s1}, α_2, and A_{s2}) of the two storage zones.

[28] Typically the conservative transport parameters are estimated first, by an inverse model run that optimizes those parameters to fit the conservative solute tracer data. The non-conservative transport parameters are then estimated by a second model run that is optimized to fit the non-conservative tracer data. The rate parameters for sediment removal also must be estimated sequentially because λ_{sed} accounts for total removal from the stream while $\lambda_{S1,sed}$, $\lambda_{S2,sed}$ each account for a proportion of the total that occurs in specific zones of the stream. Thus we could not simply estimate all three removal rate parameters in a single step because non-unique results would be expected. Instead our approach was to estimate λ_{sed} in the OTIS-2stor simulation (while setting $\lambda_{S1,sed}$, $\lambda_{S2,sed}$ to zero). This approach is valid for quantifying the sum of all processes contributing to removal. In a second step we independently estimated $\lambda_{S1,sed}$, $\lambda_{S2,sed}$ by other means using in situ data measured in the hyporheic zone (described in section 3.7.3). The remaining removal processes for fine sediment not accounted for by our in situ sampling in the hyporheic zone (e.g., settling to the streambed) could then be calculated by difference, i.e., $\lambda_{sed} - \lambda_{S1,sed} - \lambda_{S2,sed}$. The uncertainties of the estimated parameters, when expressed as coefficients of variation, are on the order of 0.1 for A, and between 0.5 and 2 for D_L, α_1, A_{s1}, α_2, A_{s2} and λ_{sed}, which is typical for environmental modeling and considered good for widely varying and poorly know parameters in natural streams. Uncertainty estimates for $\lambda_{S1,sed}$ and $\lambda_{S2,sed}$ are discussed in section 3.7.3.

[29] Additional parameters can be calculated directly from the basic parameter values. Those include mean residence time (t_s) and physical dimension (d_s) of storage zones. The mean residence time (t_s) of fluid and solute that enter the storage zones is estimated by the ratio of the storage zone cross-sectional area (A_s) and the storage-exchange flux (the product of α and A) (equation (7) in Table 1). The estimate of storage depth determined by reach scale modeling can be directly compared with in situ measurements in the streambed. Estimation of the depth of storage (d_s) assumes lateral extension across the full width of the stream. The hyporheic depth, d_h, can be computed as $A_s/(w\,\theta)$ where w is average stream width and θ is average porosity of the streambed, which must be added for calculations that are compared with in situ measurements in the hyporheic zone (equation (6) in Table 1). Methods of directly estimating mean residence times (t_h) and physical dimensions of the hyporheic zone (d_h) at small spatial scales are presented in section 3.7.3.

Table 1. Reach and Geomorphic Unit Scale Estimates of Storage and Removal of Solutes and Fine Particulates[a]

Parameter Description	Equation	Equation Number	Variables Not Previously Defined
	Reach Scale Estimates		
Depth of storage zones in surface water or streambed sediment	$d_s = \frac{A_s}{w}$	(5)	average width of stream (w), average sediment porosity (θ)
	$d_h = \frac{A_s}{w\vartheta}$	(6)	
Residence time of stream water in storage zones	$t_s = \frac{A_s}{\alpha A}$	(7)	storage zone and main flow zone cross-sectional areas (A_s and A), storage- exchange coefficient (α)
Uptake velocity of stream water into storage zones	$V_w = \frac{\alpha A}{w}$	(8)	
Removal velocity of fine particulates by all processes	$V_{sed} = \frac{\lambda_{sed} A}{w}$	(9)	first-order deposition coefficient for fine particulates in stream (λ_{sed})
	Geomorphic Unit-Scale Estimates		
Residence time of stream water in migrating bedforms	$t'_{bedform} = \frac{\lambda_{bedform}}{u_b}$	(10)	velocity of bedform migration (u_b), bedform wavelength (λ_{bedform})
Uptake velocity of stream water into migrating bedforms	$V'_{bedform} = \vartheta(H/2)\frac{u_b}{\lambda_{bed}}$	(11)	bedform height (H), i.e., vertical height of bedform from peak to trough
Uptake velocity of stream water into hyporheic zone	$V'_h = \vartheta f_{sw}\frac{d_h}{t_h}$	(12)	depth in streambed of measuring point in hyporheic zone (d_h), fraction surface water (f_{sw}) in subsurface sample determined from Br tracer, median residence time of solute tracer at sampling depth (t_h)
Removal velocity of fine particulates in hyporheic flow paths	$V'_{h,sed} = (C_{sw}f_{sw} - C_h)/C_{sw})V'_h$	(13)	plateau concentration of fine particulate tracer in surface water (C_{sw}), plateau concentration in hyporheic zone (C_h), fraction surface water (f_{sw}) in subsurface sample determined from Br tracer, uptake velocity of stream water into hyporheic zone (V'_h)

[a]Note that reach scale parameters are not specific about where storage or removal occurs in a stream, whereas geomorphic unit scale estimates are specific about the location of storage or removal. Variables are defined in order presented.

Table 2. Summary of Flow and Geomorphic Conditions at Downstream End of the Experimental Reach in Clear Run, N.C. During Base Flow and Flood[a]

Flow Condition	Stream Width (m)	Stream Depth (cm)	Stream Velocity (cm s^{-1})	Stream Discharge (m^3 s^{-1})	Bedform Height (cm)	Bedform Wavelength (cm)	Bedform Migration Rate (cm min^{-1})	Sand Grain Diameter (μm)
Base flow	3.1 ± 0.3	6	17–21	0.06	1	12	0.9 (0.2–1.7)	380 ± 30
Flood peak	3.5 ± 0.5	20	32–49	0.39	3	75	11.3(10.5–11.9)	n.a.

[a]Values are means and standard deviations, except water velocity which is reported as a range and bedform migration rate, which is reported by a mean followed by a range in parentheses.

3.7.3. Comparison of Reach- and Geomorphic Unit-Scale Estimates of Tracer Dynamics

[30] We used uptake velocity as a simple and general expression of the exchange flux of stream water with storage zones, or alternatively, the removal flux of solute or fine particles (Table 1). Using a common expression allowed us to compare tracer dynamics across spatial and temporal scales. The term "storage" denotes a temporary delay in transport resulting from exchange between the main channel and relatively slowly flowing zones of the stream, such as recirculating flow of surface water or flow through hyporheic paths. Tracer that is still stored at the end of the experiment is referred to as having been "removed" from the flowing stream water. It is recognized that longer timescale storage can occur (e.g., in very long hyporheic flow paths) and that changing flow conditions can quickly remobilize stored tracer. For that reason we focused on quantifying storage and removal rates of solutes and particles at base flow followed by a flood to determine the extent to which tracer "removed" during base flow might suddenly be entrained. To improve our interpretations of the physical processes involved we compared reach-scale uptake velocities estimated from in-stream tracer data with estimates of specific storage processes measured in situ (e.g., migrating bedforms or hyporheic flow). The comparison aids in evaluating the relative importance of specific storage and removal processes.

[31] Uptake velocities directly estimated at the scale of the stream reach are summarized in equations (8) and (9) in Table 1. Reach-scale uptake velocities were calculated by multiplying the best fit rate parameters from OTIS-2stor simulations (i.e., α for water or conservative solutes or λ for fine particulates) by the average stream depth (Table 1). For example, V_w is the reach-averaged uptake velocity at which water enters the dominant storage zones, which may include storage in slowly moving surface or subsurface water. Likewise, V_{sed} is the reach-averaged uptake velocity describing the net rate of removal of fine particulates from streamflow by all processes, including flocculation, settling, and advective transport into and filtration within hyporheic flow paths.

[32] Some uptake velocities associated with specific geomorphic features could be directly estimated using local in situ observations. Those calculations are summarized in equations (10)–(13) in Table 1. The uptake velocity associated with turnover of migrating bedforms, $V'_{bedform}$ (equation (11) in Table 1) was estimated using measurements of the celerity of migrating bedforms (u_b), average bedform wavelength (λ_{bedform}), bedform amplitude (h_m), i.e., the height difference between bedform peak and mean bed height, and streambed sediment porosity (θ). Average fluid residence time in actively migrating bedforms ($t'_{bedform}$) was calculated using the same measurements (equation (10) in Table 1). It should be noted that $V'_{bedform}$ applies both to solute and suspended particulates because mobile bedforms store and release both constituents at the same rate as long as fine particulates are entrained into streamflow when re-exposed by bedform turnover [*Packman and Brooks*, 2001]. Note that all geomorphic unit-scale uptake velocities are distinguished from their reach-scale counterparts using a prime superscript for symbols.

[33] Another uptake velocity that could be directly estimated from field data was solute uptake into hyporheic flow paths, V'_h. Solute uptake in hyporheic flow was directly estimated using measurements of streambed sediment porosity (θ), the median tracer travel time, t'_h, depth to the sampling point in the streambed sediment (d_h), and the fraction of surface water in hyporheic flow paths at the measurement depth that was derived from the stream (f_{sw}) (equation (12) in Table 1). The median travel time of the solute tracer was estimated based on the time that subsurface concentration reached 50% of its eventual plateau value at the sampling depth. The fraction of hyporheic flow derived from the stream was computed as $(C_s - C_h)/(C_s - C_b)$ where C_s and C_h are the observed tracer plateau concentrations in the stream and hyporheic zone, respectively, and C_b is the background tracer concentration. Note that results are reported for all depths (1.4, 2.9, 4.9, and 7.9 cm) where hyporheic flow was detected.

[34] Last, the uptake velocity of fine particulate removal by filtration in hyporheic flow paths, $V'_{h,sed}$, was directly estimated using equation (13). The approach for estimating uptake of fine particulates follows from *Triska et al.* [1989] and *Harvey and Fuller* [1998] and builds on equations for conservatively transported solutes in hyporheic flow paths with an additional parameter for removal (equation (13)). Previous method testing by *Harvey and Fuller* [1998] indicates that uncertainties are expected on the order of 3% for this method.

4. Results

4.1. Hydrologic and Geomorphic Conditions During Base Flow

[35] During base flow Clear Run is a shallow (6 cm) and fast moving (20 cm s^{-1}) sand-bed stream with primary roughness created by flow over dune-shaped sandy bedforms. There also were no systematic longitudinal trends in channel features or grain size distributions that were apparent in the experimental reach. The average hydraulic conductivity of the streambed was 0.048 cm s^{-1} ± 0.008 and the average porosity was 0.4. Other characteristic measurements of streamflow and morphology are noted in Table 2.

[36] Grain size distributions at Clear Run were unimodal with a median diameter (D_{50}) of 340 μm on bedform crests

Table 3. In-Stream Mass Balance of Solute Tracer (Bromide) and Fine Particulate Tracer at Downstream End of the Study Reach (Site S2)[a]

Mass Balance Term	Br Tracer (%)	Fine Particulate Tracer (%)
Tracer transport during base flow		
Mass transported in stream	99 ± 2	29
Mass stored or removed from stream	1	71
Tracer entrained by flood		
Mass detected in flood flow	0.2	21
Retention of tracer after flood	<1	50

[a]Mass is expressed as a percentage of the total mass injected into the stream for 3.5 h during base flow. Uncertainty in recovering the entire injected solute tracer was just ±2%, which is excellent for an environmental tracer. The mass balance shows that very little solute tracer was stored during base flow, whereas a substantial proportion of the fine particulate tracer was stored (71%). Approximately thirty percent of the stored particles (21% of the total injected mass) were rapidly entrained back into the stream by the flood. In contrast, approximately seventy percent of the stored particles (50% of the total injected mass) were retained rather than flushed from the stream reach by the experimental flood.

and a median diameter of 370 μm in the troughs of bedforms. Grain-size variability on bedform crests was slight with sand ranging from a 10th percentile grain diameter (D_{10}) of 210 μm to a 90th percentile grain diameter (D_{90}) of 600 μm. The D_{10} in bedform troughs was the same as crests (210 μm) however the D_{90} was larger (960 μm) in troughs due to sorting of the sand during bedform migration, when coarse sediment grains mobilized from crests and then were preferentially captured in the small avalanches that collapsed down the lee faces into troughs.

[37] Bedforms had an average height at the crest of 1 cm and wavelength of 11.8 cm during base flow. The migration rates of bedforms averaged 0.016 cm s^{-1} but exhibited strong spatial heterogeneity with rates ranging from 0.003–0.029 cm/s. The measured distribution of bedform wavelengths was closely approximated by a gamma distribution with shape parameter of 3.53 cm and scale parameter of 3.35 cm. Measured profiles of natural particulate organic carbon from streambed cores confirmed that organic carbon was present in low quantities, with a tendency to exhibit a peak value (with an average of 0.6% carbon by weight) at a depth of 2–4 cm. Above and below that depth carbon percent was six times lower (0.1%).

4.2. Solute and Fine Particulate Transport Dynamics During Base Flow: Modeling of Reach-Scale Transport and Storage

[38] Mass balance closure of the conservative solute tracer bromide was achieved in this stream tracer experiment. Within the overall uncertainty of the solute mass balance (±2%), essentially all tracer (99%) was accounted for in downstream sampling (Table 3). After the injection started the bromide tracer concentration rapidly increased and within tens of minutes reached a plateau on which it remained until three and a half hours had elapsed and the injections were stopped. When the injection was stopped the bromide concentration decreased rapidly for tens of minutes as bromide was flushed out of the experimental reach through the main channel. Bromide concentration then declined much more slowly for the remainder of the experiment as the tracer was flushed from storage zones. In contrast, the fine particulate tracer was highly non-conservative in its transport, with 71% of the fine particles being removed in the 221 m experimental reach during base flow compared to less than 1% removal of bromide in the same reach (Table 3).

[39] Reach-scale modeling using OTIS-2stor indicated a relatively small value of longitudinal dispersion (D_L approximately 0.2 m^2 s^{-1}), which was consistent with the morphology of Clear Run. In addition, the modeled exchange of water and solute between the main channel and storage areas indicated that those storage areas were relatively small, accounting for an accumulated storage area approximately twenty percent of the complete stream area (Table 4).

[40] Fine particulates were non-conservatively transported, as indicated by the breakthrough of the fine particulate tracer which both lagged and was attenuated relative to the solute tracer (Figure 6). Two OTIS-2stor simulations are shown in Figure 6, one assuming that particulates were transported conservatively and the other assuming a first-order irreversible removal process. The model with removal better accounted for the net effect of removal processes, as indicated by the lower plateau in tracer concentrations that more closely matched the measurements. The fitted first-order removal term indicated a net removal of fine particulates at a rate of 0.002 cm s^{-1} (equation (8) in Table 1). There remains, however, a significant lack of model fit, both on the rising shoulder of the fine particulate breakthrough curve and on the plateau. One reason for the imperfect model fit is that the fine particle data are noisy, which may reflect actual variability or may reflect a greater error in sampling and quantization. The systematic lag of fine particulate concentrations behind the simulation on the rising limb of the breakthrough curve (Figure 6) is an underestimation of storage exchange of fine particulates due to estimating the storage-exchange processes by the bromide tracer fit, which will be discussed later. Also there is a clear lack of fit at the time of arrival of the experimental flood because no attempt was made to directly simulate flood dynamics. Entrainment of fine particles by the flood is discussed in section 4.4.4.

Table 4. Best Fit Parameters Determined for OTIS-2stor Simulations of Solute and Fine Particulate Tracer Transport at Base Flow in the Experimental Reach

Parameter	Unit	Reach 1: Injection to Site S1 (47 m)	Reach 2: Site S1–S2 (174 m)
$Q_{Average}$	m^3 s^{-1}	0.0589	0.0681
A	m^2	0.235	0.296
D_L	m^2 s^{-1}	0.02	0.19
A_{S1}	m^2	0.038	0.030
A_{S2}	m^2	0.023	0.020
α_1	1/s	2.48E-03	3.00E-04
α_2	1/s	1.13E-04	2.00E-05
q_L^{in}	m^2 s^{-1}	3.75E-05	3.75E-05
q_L^{out}	m^2 s^{-1}	0	0
C_L	mgL^{-1}	0.0353	0.0353
λ_{sed}	1/s	3.0 E-03	4.0 E-04
$\lambda_{S1\text{-}sed}$[a]	1/s	0	0
$\lambda_{S2\text{-}sed}$[a]	1/s	0	0

[a]Storage-zone reaction parameters set to zero for reach-scale optimization (see explanation in text).

Table 5. Spatially Averaged Vertical Exchange of Water, Solute, and Fine Particulates and Removal Fluxes of Fine Particulates[a]

Parameter Name	Symbol	Base Flow Value	Flood Value	Unit	Equation
Reach scale					
Uptake velocity into OTIS-2stor storage zone 1	V_{w1}	1.8E-03	na	cm s^{-1}	(8)
Uptake velocity into OTIS-2stor storage zone 2	V_{w2}	1.2E-04	na	cm s^{-1}	(8)
Geomorphic unit scale					
Uptake into migrating bedforms, hyporheic					
Upper	$V'_{bedform}$	2.7E-04	1.5E-03	cm s^{-1}	(11)
Uptake in "middle" hyporheic					
1.4 cm	$V'_{h,\ 1.4}$	8.5E-04	na	cm s^{-1}	(12)
2.9 cm	$V'_{h,\ 2.9}$	8.3E-04	na	cm s^{-1}	(12)
4.9 cm	$V'_{h,\ 4.9}$	6.7E-04	na	cm s^{-1}	(12)
Uptake in "lower" hyporheic					
7.9 cm	$V'_{h,\ 7.9}$	4.4E-05	na	cm s^{-1}	(12)
Removal Flux of Fine Suspended Particles					
Reach scale					
Suspended particle removal by all processes	V_{sed}	2.4E-03	na	cm s^{-1}	(9)
Geomorphic unit scale					
Fine particle removal in middle hyporheic					
1.4 cm	$V'_{h,sed,\ 1.4}$	5.7E-04	na	cm s^{-1}	(13)
2.9 cm	$V'_{h,sed,\ 2.9}$	7.5E-04	na	cm s^{-1}	(13)
4.9 cm	$V'_{h,sed,\ 4.9}$	2.2E-05	na	cm s^{-1}	(13)
Fine particle removal in lower hyporheic					
7.9 cm	$V'_{h,sed}$	no detect	na	cm s^{-1}	(13)

[a]All fluxes are expressed as uptake fluxes, i.e., the depth of stream water per time that is exchanged with the streambed (or the depth of stream water per time from which fines are removed).

4.3. In Situ Measurements Beneath Bedforms: The Geomorphic Unit Scale

[41] During base flow, a combination of hyporheic exchange and turnover by bedform migration led to rapid storage-exchange in the shallow streambed. The uptake associated with bedform migration was fast, 2.7 E-04 cm s^{-1} but exchange caused by hyporheic flow was even faster (8.5E-04 cm s^{-1} at 1.4 cm deep). Thus, hyporheic flow and bedform migration were both important exchange processes during base flow. The resulting mean residence time of pore water in the top 1.5 cm of streambed was slightly more than 10 min indicating that exchange occurred fast enough that tracer concentrations in the shallow subsurface lagged only slightly behind changes in concentration that occurred in the stream.

[42] Solutes were transported more slowly into hyporheic flow paths beneath the layer of active bedform migration. Whereas the uptake velocity was dominated by a combination of hyporheic exchange and bedform turnover in the uppermost 0.5 cm of the hyporheic zone, only hyporheic exchange was operative below this depth. The hyporheic flux declined with depth in the streambed, especially below 5 cm (Table 5) and reached a maximum penetration depth of 8 cm (Figure 7). Uptake velocities of 8.5E-04 and 8.3E-04 cm s^{-1} were similar at shallow depths (1.4 and 2.9 cm, respectively), followed by a slight decline at 4.9 cm (6.7 E-04 cm s^{-1}), and then a precipitous decline by more than an order of magnitude at 7.9 cm deep (4.4E-05 cm s^{-1}). The corresponding median residence times were 11 and 16 min in the middle hyporheic zone (1.4 and 2.9 cm deep), and were considerably greater at deeper depths, i.e., 44 min at 4.9 cm deep and 120 min at 7.9 cm deep (Table 6).

[43] Fine particulates also entered the streambed with hyporheic flow but, due to filtration, only propagated to a maximum depth of approximately 60 percent of the depth of solute penetration, i.e., 4.9 cm for fine particulates compared

Table 6. Depth of Storage Zones and Residence Times of Water and Solute

Parameter Name	Symbol	Base Flow Value	Flood Value	Unit	Equation
Reach scale					
Depth - OTIS-2stor storage zone 1 in sediment	$d_{s\text{-}upper}$	3	na	cm	(5)
Depth - OTIS-2stor storage zone 2 in sediment	$d_{s\text{-}lower}$	2	na	cm	(5)
Plot scale					
Bedform height – crest to trough	H	1.0	3.3	cm	na
Depth - upper hyporheic beneath bedforms	$d_{h\text{-}upper}$	3	na	cm	(6)
Depth - lower hyporheic beneath bedforms	$d_{h\text{-}lower}$	2	na	cm	(6)
Water and Solute Residence Times in Storage					
Reach scale residence times					
OTIS-2stor_storage zone 1	$t_{s\text{-}1}$	5	na	min	(5)
OTIS-2stor_storage zone 2	$t_{s\text{-}2}$	56	na	min	(5)
Geomorphic-unit scale residence times					
Migrating bedforms (includes upper hyporheic)	$t'_{bedform}$	0.5	0.37	min	(9)
Middle Hyporheic (1.4, 2.9, 4.9) cm beneath bedforms	$t'_{h\text{-}middle}$	11, 16, 44	na	min	na
Lower Hyporheic (7.9 cm) beneath bedforms	$t'_{h\text{-}lower}$	120	na	min	na

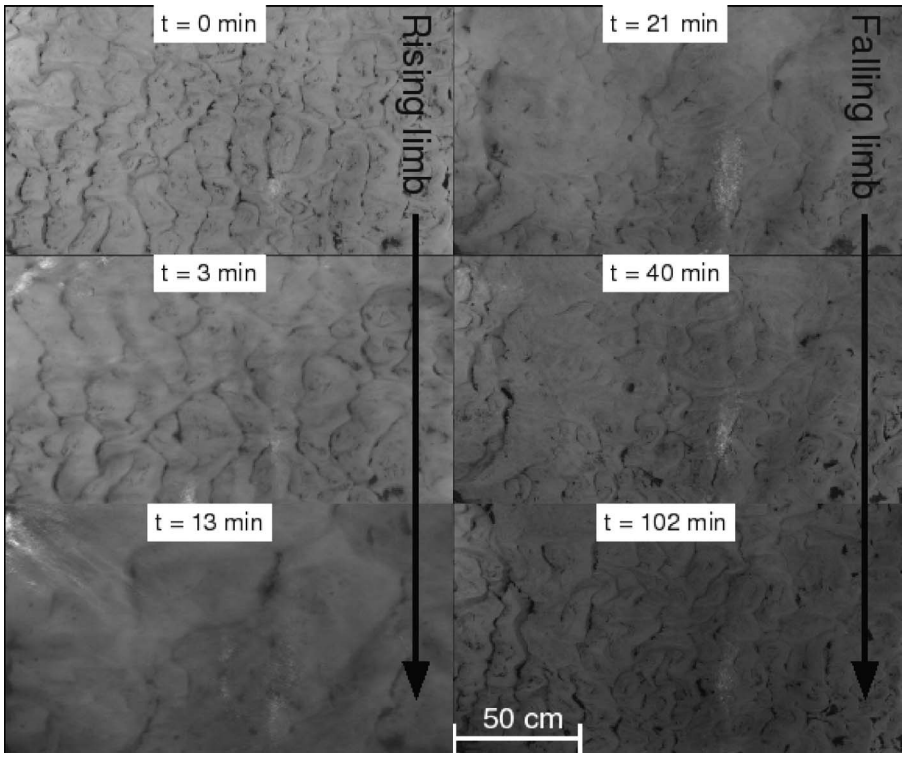

Figure 4. Overhead photographs of streambed evolution through the flood. The time indicated with each photo is relative to when the flood was released, which occurred 4.5 h after the tracer injections began.

with 8 cm for solute. Filtration was strongest at shallow depths beneath the streambed. The estimated uptake rates for fine particulates in hyporheic flow paths beneath bedforms were 5.7E-04 at 1.4 cm deep, 7.5E-04 at 2.9 cm deep. Between 3 and 5 cm the uptake rate for fine particulates decreased by an order of magnitude (i.e., 2.2E-05 at 4.9 cm deep).

4.4. Flood-Induced Temporal Dynamics of Solutes and Fine Particulates

4.4.1. Flood Dynamics

[44] The dam release occurred 4.5 h after the start of the tracer injections, and the flood was first observed 7.5 min later at the bedform photo-imaging and hyporheic measurements site location. Stream discharge rose very steeply and reached a peak (390 L/s) at 17.5 min after the dam release. At the time of the flood peak the stream depth and velocity had approximately tripled and doubled, respectively (Table 2). A more gradual recession back to base flow followed the flood peak that lasted for another 22 min. The flood had completely passed the photo-imaging and hyporheic measurement site at 38 min after the dam release. Accompanying the flood was a minor amount of bank storage, which was limited by the small rise in stream water level and by the short duration in the flood (results not shown, discussed further in section 4.4.2).

4.4.2. Flood-Induced Geomorphic Changes

[45] The bedforms began to grow nearly instantaneously with the flood's arrival, and within ten minutes had grown from 1 cm high by 12 cm long dune-like bedforms migrating downstream at a rate of 0.016 cm s^{-1} to 3 cm high by 75 cm long dune-like bedforms migrating at 0.19 cm s^{-1} (Figure 4). Celerities of bedform migration were more uniform during the flood, with a much narrower relative range (0.17–0.20 cm s^{-1}) during the flood compared with base flow (0.003–0.029 cm s^{-1}).

[46] In contrast to the rapid growth of large bedforms on the flood's rising limb, the flood-created bedforms changed much more slowly to re-form smaller bedforms. First, larger bedforms rapidly became frozen in place as the flood discharge declined, followed by the growth and migration of smaller bedforms on the backs of larger bedforms, which eventually consumed the larger bedforms by shaving off the tops and filling the troughs. This process of replacing flood-created bedforms with smaller, pre-flood bedforms required approximately 95 min from the time of the flood peak, which was almost five times longer than the time it took for the flood's recession. See Movie S1 in the auxiliary material to view the complete set of photographic images that illustrate the effect of the experimental flood on sand ripples.[1]

4.4.3. Flood-Induced Solute Dynamics

[47] Just prior to the flood (one hour after tracer injections stopped) the tracers had been flushed from the main channel and concentrations were low and declining very slowly due to the slow release of tracers from storage zones. We were interested in whether the flood would enhance the flushing of stored tracer or whether it would drive the tracer even deeper into storage. Storage dynamics can be assessed several ways. One way is by examining the "tail" of the in-stream solute tracer breakthrough curve for unusual flushing behavior. Before using the breakthrough curve for this purpose the data

[1]Auxiliary materials are available in the HTML. doi:10.1029/2012JG002043.

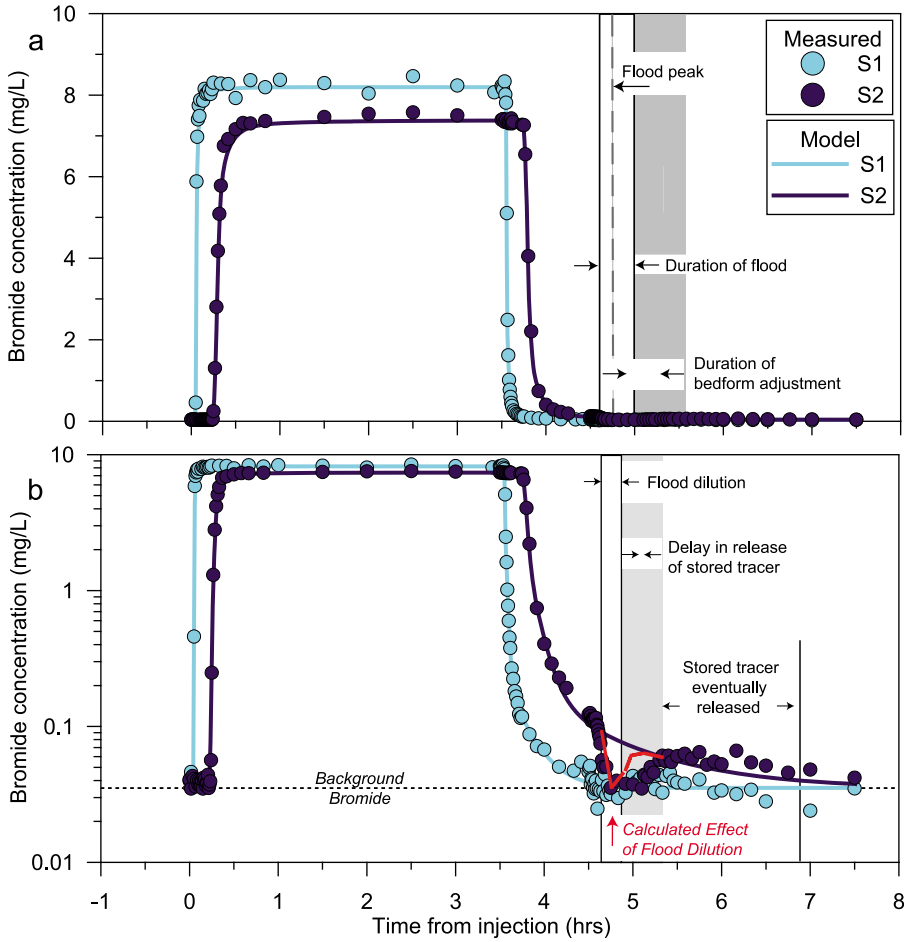

Figure 5. Solute tracer measurements and best fit OTIS-2stor simulation of conservative solute transport. Data and simulations are shown on (a) linear and (b) logarithmic scales with markers added to denote the timing of the experimental flood and associated dynamics. The OTIS-2stor model simulations assume solute dynamics without flooding, whereas the model simulation in red is a calculation that accounts for flood dilution of the tracer at site S2. Comparison with S2 data indicates that the tracer was diluted briefly during the flood, followed by a period where the return of stored tracer from subsurface storage zones was delayed (i.e., measured tracer was substantially lower than what could be accounted for by dilution). After the flood passed and also after storm-created bedforms had begun to revert to pre-flood dimensions, the stored tracer was finally released from delayed storage flow paths en masse, causing a second peak in concentration in Figure 5b. The time period of flood affected tracer dynamics lasted approximately twice as long as the time period for bedforms to fully readjust to pre-flood conditions.

needed to be normalized to remove the effect of tracer dilution during the flood. We used a simple equation to estimate the normalized in-stream bromide concentration that discounted the dilution effect of mixing with floodwater with the background concentration of tracer:

$$C_{dil}(t) = \frac{(Q_{flood}(t) - Q_b)}{Q_{flood}(t)} C_b + \left(\frac{Q_b}{Q_{flood}}\right) C_{model}(t), \qquad (4)$$

where C_{dil} (t) is the diluted in-stream solute tracer concentration measured at time t during the flood, C_b is the background solute tracer concentration of flood water, C_{model} (t) is the undiluted OTIS-2stor prediction of solute tracer concentration for base flow conditions, Q_{flood} (t) is the measured flood discharge, and Q_b is the base flow discharge.

[48] The effect of dilution is clearly shown in Figure 5b. Initially dilution explains the dip in measured in-stream concentrations. However, dilution cannot explain the continuation of lower than expected values of tracer concentrations lasting for 30 min after the flood had recessed to base flow (Figure 5b). We interpret the delay in flushing during and after the flood as a result from tracer driven deeper into storage. The in-stream bromide tracer concentration eventually began to rise again, ultimately reaching a "second peak" in tracer concentration, which was a very low second peak concentration, although nonetheless something that is rarely seen in stream tracer experiments (Figure 5b). The second peak lasted approximately one hour, which is inferred to be the time period required for tracer that previously was delayed in storage to be flushed. The delayed storage lasted 120 min past the flood's arrival, as judged by the time required for the in-stream bromide to return to the expected pattern of slowly declining concentration at base flow (Figure 5b). The delay in storage may have lasted longer than

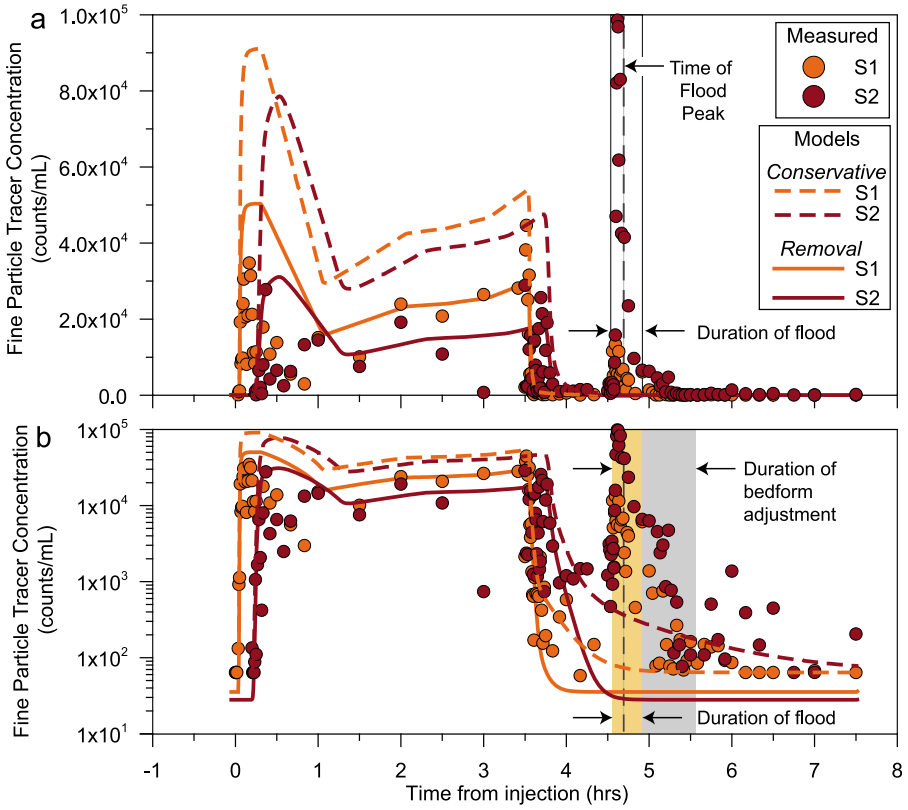

Figure 6. Fine particulate tracer measurements and best fit OTIS-2stor simulation of transport and removal of fine particulates during base flow. Results are plotted on (a) linear and (b) logarithmic concentration scales for comparison. The duration of the flood's passage is denoted by the orange bar and duration of adjustment of flood-created bedforms is denoted by a gray bar. No attempt was made to directly simulate the flood's effect on transport. In contrast with the solute tracer, for which the effect of the flood was a delayed tracer release from storage, the fine particulate tracer was rapidly entrained on the rising limb of the flood.

2 h but would not be discernable in the in-stream tracer data due to the very low levels of tracer signal above a background concentration that typically has a 10 to 20% uncertainty.

[49] Solute tracer flushing from hyporheic flow paths was delayed for at least 30 min after the flood recessed. The timescale of the delay was similar to the time that large, flood-created bedforms persisted. Deeper hyporheic exchange was expected beneath these larger bedforms, and that inference was supported by observing that the hyporheic zone deepened from 8 cm at base flow to 15 cm beneath the flood peak [*Bhaskar et al.*, 2012]. Although bank storage also commonly occurs during floods, our measurements in the stream bank at Clear Run indicated that the extent of bank storage during the small experimental flood was nil. Hydraulic head measurements in the stream and stream bank made by a University of North Carolina-Wilmington scientist (Eric Henry, personal communication, December, 2009) indicated that moderate bank storage may have occurred. At the peak of the flood the stream stage had increased from 6 to 20 cm, a rise of 14 cm, although the head increase was substantially attenuated (by 7 cm) at a distance 2 m into the bank. Most importantly we observed no significant movement of stream tracers into the bank within our bank samplers. These observations substantiate that storage dynamics with this small flood were mainly the result of vertical interactions beneath bedforms rather than lateral interactions with the steam bank. Larger floods could produce a different result with greater importance of bank storage.

4.4.4. Flood-Induced Fine Particulate Dynamics

[50] The flood had a dramatic and immediate effect on entraining the fine particulate tracer from the streambed (Figure 6). Thirty percent of the fine particulate tracer that had been removed from stream water during base flow was rapidly entrained in a large pulse on the rising limb of the flood (Table 3 and Figure 6). Storm-created bedforms scoured the bed to an average depth of 1.5 cm, i.e., 1/2 the average bedform height of 3 cm. We expected that all of the fines that were deposited during base flow would be mobilized by the flood. Instead we found that only 69% of the tracer that was deposited during base flow remained in storage after the flood (Table 3, i.e., 21% of the total injected mass of fine particles was entrained, divided by 71% that was deposited equals 31%). Approximately half of that (35%) is accounted for by fines that penetrated deep enough (i.e., below 1.5 cm) to escape entrainment, but the fate of the other 34% of the tracer retained after the flood is not known. Possibilities include additional filtration in deeper, flood-created hyporheic flow paths or removal elsewhere in an unaccounted for storage zone. For example, after the flood some of the particulate tracer was observed stuck on the bank and

on overhanging vegetation that had been submerged during the flood, which may have been an important removal mechanism. Unfortunately we did not sample the bed by coring after the flood, which in hindsight was a mistake because such measurements have the potential to distinguish between the three alternatives. Future efforts would benefit by directly sampling the bed by coring at the end of such experiments.

5. Discussion

5.1. Solute Storage-Exchange During Base Flow

[51] Our tracer experiments at Clear Run focused on identifying the dominant processes and relative timescales of storage-exchange during base flow and readjustment by a flood. In situ observations in specific geomorphic units ranged widely (over three orders of magnitude) and were generally less than the uptake velocities determined from reach-scale modeling of the in-stream tracer signal (Table 5). Finding higher values of uptake velocities in reach-scale modeling is consistent with this approach being better suited to characterize the faster storage-exchange processes [*Harvey and Wagner*, 2000].

[52] A comparison between reach-scale and in situ measurements indicated that reach-scale modeling was sensitive to hyporheic exchange. The physical dimensions of the model-inferred storage zones (several cm accounting for streambed sediment porosity) were similar to the measured depth of hyporheic flow. Also, the model-inferred residence times of storage (minutes to tens of minutes) were similar to those measured in situ. The faster exchanging storage zone (storage zone 1) appears to have characterized very rapid hyporheic flow just beneath bedforms as suggested by a residence time (5 min) that was approximately half of the 11 min residence time measured at 1.4 cm. Storage zone 2 had a residence time that best matched the measured residence time of hyporheic flow at 4.9 cm deep.

[53] On the other hand, there is likely to have been some blending of signals in the reach scale modeling. For example, the in situ estimates of bedform turnover and hyporheic exchange in Table 5 have similar timescales, and were likely detected as a blended signal by reach-scale modeling. Also, neither of the reach-scale storage zones matched the much slower exchange occurring through deeper (5–8 cm) hyporheic flow paths. Thus there were components of storage that were too slow to be detected by reach-scale modeling of the in-stream tracer dynamics. Similarly, there were storage processes that were too fast to be detected as a storage-exchange process in reach-scale modeling. For example, very fast storage-exchange occurring with surface zones of flow separation within bedforms troughs was not detectable. Very fast storage exchange (1 min or less) would have achieved equilibrium mixing conditions after a short distance of transport (<50 m) and therefore would most likely have been detected by modeling at the reach-scale as a component of longitudinal dispersion [*Wagner and Harvey*, 1997].

[54] It is also worth noting that characteristics of hyporheic flow at Clear Run were predictable based on theoretical scaling calculations. For example, the maximum depth of hyporheic flow at base flow (8 cm) agreed well with theoretical scaling for sandy streambeds with dune bedforms, where the penetration depth is approximately 80% of the dune's wavelength [*Cardenas and Wilson*, 2007; *Boano et al.*, 2007]. Also, the measured hyporheic flux beneath bedforms (0.0013 cm s^{-1}) agreed within a factor of 2 of a predicted value (0.0023 cm s^{-1}) using the scaling equation of *O'Connor and Harvey* [2008] based on laboratory and field measurements of shear stress, bedform height, and hydraulic conductivity of the streambed. This comparison with theory emphasizes the potential for predicting hyporheic flow, especially in streams with simple and well studied geomorphology such as Clear Run, where roughness is dominated by sandy, dune-shaped bedforms.

5.2. Fine Particulate Removal During Base Flow

[55] In contrast to solutes, fine particulates were highly non-conservative and were substantially removed during base flow. Seventy-one percent were removed from in-stream during an average travel time of ten minutes through the 221-m experimental reach. Filtration of fines in hyporheic flow paths accounted for approximately one-third (35%) of the total removal of fine particulates (Table 5 and Figure 1). These results suggest a significant role for the hyporheic zone in removing fine particulates in sand-bed streams. Filtration limited the depth of penetration of fines in the bed (4.9 cm compared with 8 cm for the conservative solute, Figure 7). However, even with filtration restricting the depth of penetration, fine particulates were still carried beneath the depth of physical turnover of the streambed by migrating bedforms during base flow. Tracer particles trapped by filtration below the layer of bedform turnover were not entrained until migrating bedforms grew in size during the flood or until localized scour occurred (section 5.3.3). The importance of fine particulate penetration below the level of active bedform migration is a potential enhancement of chemical reactions involving FPOM.

[56] Although fines were deposited by several processes, bedform migration was essentially the only process of re-suspension of fines during base flow. Fine particulates exchange between the stream and migrating bedforms, associated with the turning over a thin (0.5 cm) layer of the streambed, was very rapid (2.7 E-04 cm s^{-1} (Table 5). The resulting uptake velocity was intermediate between the faster (shallow) hyporheic exchange and slower (deeper) hyporheic exchange. Bedform migration therefore contributes to quickly establishing equilibrium between the stream and pore water within the region of active bed load sediment transport. The non-permanent removal or release of particulates due to migrating sand bedforms is supported by laboratory flume studies by *Packman and Brooks* [2001] and *Rehg et al.* [2005].

[57] Removal of the other two thirds of the fine particulate tracer was not directly observable but was inferred to have occurred by settling in troughs between bedforms. Settling behavior is strongly dependent on particle size. The potential importance of settling of fines at Clear Run is supported by the similarity between the reach-scale uptake velocity, 2.4 E-03 cm s^{-1} (equation (9) in Table 1), and Stokes settling velocities ranging between 1.6E-03 cm s^{-1} and 3.1 E-02 cm s^{-1} calculated for 5-μm and 20 μm particles, respectively, based on a particle density equivalent to our tracer. Preferential settling in troughs between bedforms would have occurred due to the slower velocities in the recirculating flow. Our inference is also supported by direct

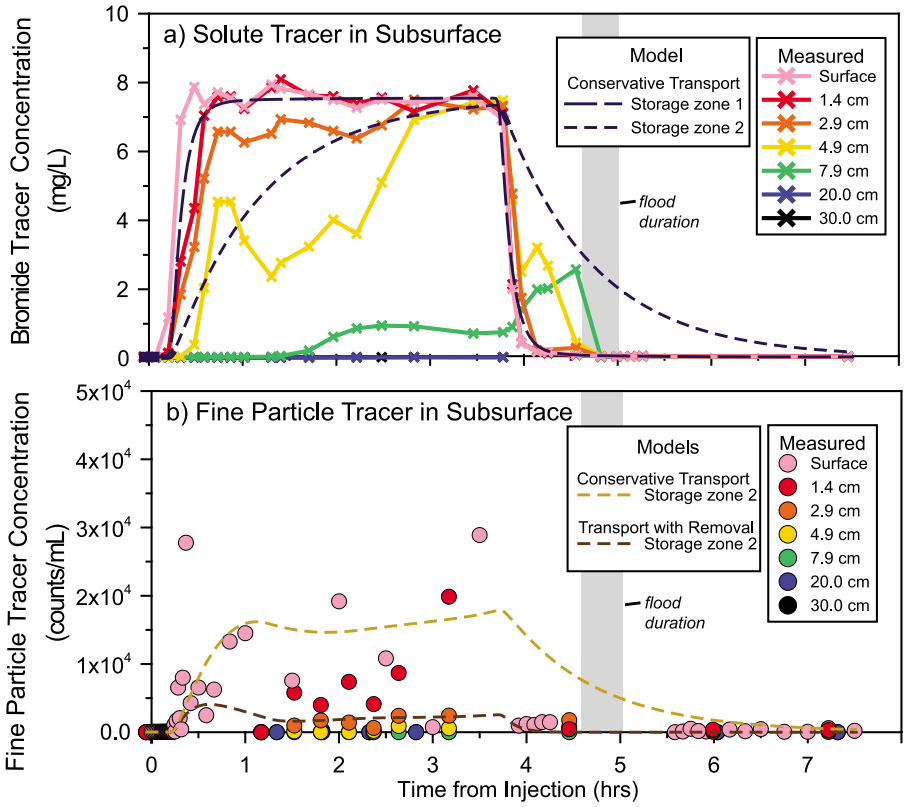

Figure 7. Observed tracer transport in hyporheic flow paths contrasted with best fit OTIS-2stor simulations of tracer storage. (a) Bromide below bedforms and (b) fine particulate tracer below bedforms. No attempt was made to directly simulate effects of the flood.

observations using time-lapse photography showing the collection and retention of CPOM naturally in bedform troughs (Figure 4). Movie S1 is produced from photography and shows that trapped CPOM is shuttled downstream with migrating bedforms. Movie S1 also suggests that POM may occasionally be buried by advancing crests or ejected back into the main flow due to random turbulent bursts that penetrate into troughs (see Figure 1). We propose that all of these processes may have affected the fine particulate tracer.

5.3. Flood Effects: Differential Dynamics of Solutes and Fine Particulates

5.3.1. Bedform Dynamics During the Flood

[58] During the flood the stream velocity approximately doubled (from 20 to 40 cm s^{-1}), which increased boundary shear stress and streambed sediment transport due to the higher migration rate of bedforms (from 0.016 to 0.19 cm s^{-1} during the flood peak). The greater depth of flood flow (20 cm deep compared with 6 cm deep during base flow) permitted the sandy bedforms in Clear Run to grow in height (from 1 to 3 cm) and wavelength (from 12 to 75 cm). Those geomorphic responses to the flood are consistent with many observations in sand-bed streams [e.g., *Allen*, 1973]. Our experimental flood was very short-lived, however, lasting just one half hour before stream discharge completely recessed to base flow. Figure 4 shows that bedforms recovered more slowly than discharge, with approximately 2 h required for smaller bedforms to replace larger ones. The transient lag in bedform response to changes in stream discharge has previously been observed [*Wilbers and Ten Brinke*, 2003; *Gee*, 1975]. Movie S1 shows in unprecedented detail for a field study that the lag for recovery involves the growth and migration of smaller bedforms over larger ones that eventually consume the larger bedforms. As the flood wave recedes, the large bedforms cease to migrate and became relict features. Smaller bedforms form on the backs of larger ones, with migration of the smaller bedforms eventually consuming the larger relict features (Martin and Jerolmack, submitted manuscript, 2012). The manuscript documents transient responses of bedforms in a flume and models a period of bedform growth during the rising limb of the hydrograph caused by a collision and merger process that forms larger bedforms. On the falling limb, small bedforms form on the backs of larger bedforms that have become frozen in place. Smaller bedforms fill the troughs between larger bedforms until only small bedforms remain, a process that Martin and Jerolmack (submitted manuscript, 2012) refer to as "cannibalization." Importantly, Martin and Jerolmack (submitted manuscript, 2012) found that readjustment often takes much longer than growth of large bedforms, with timescales depending on relative bedform volumes and the relative bedform migration rates at low and high discharges.

5.3.2. Solute Dynamics During the Flood

[59] The delayed flushing that we observed at Clear Run was the result of the flood peak driving tracer deeper into storage zones. According to theory, the larger bedform dimensions and greater stream velocity during the flood would increase hyporheic exchange and deepen hyporheic

flow paths [*Elliott and Brooks*, 1997; *Cardenas and Wilson*, 2007], with hyporheic flow as deep as 60 cm predicted for the maximum wavelength of flood-formed bedforms of 75 cm. We directly measured deepening of hyporheic flow at Clear Run [*Bhaskar et al.*, 2012]. The pressure gradients that drive hyporheic flow should respond nearly instantaneously to changes in bed morphology but the timescale of solute transport along these new flow paths is much longer. Therefore, the flood activated deeper hyporheic flow paths but the flushing of those paths with stream water was effectively muted by the short-lived duration of flooding and relatively rapid recovery of pre-flood bedforms. The relative timescales of geomorphic perturbations in bed morphology and transport timescales of hyporheic flow were shown to be the key controls on flood dynamics of the hyporheic zone.

[60] The dynamic expansion of hyporheic flow during the flood was extended by the hysteresis in bedform response. The adjustment of flood-created bedforms back to pre-flood dimensions lasted more than four times longer (95 min) than the flood's recession (22 min). However, even more time would have been needed to fully flush hyporheic flow paths beneath the flood-created bedforms (estimated to be on the order of 10 h). Since floods typically only last for a few hours in small streams subjected to flashy runoff, the dynamic expansion of hyporheic flow paths is most likely to be muted in small streams. On the other hand, flow velocities and bedforms are larger in big rivers [*Carling et al.*, 2000; *Nittrouer et al.*, 2008] and could produce more persistent bedforms. Martin and Jerolmack (submitted manuscript, 2012) estimated bedform adjustment times for floods in several rivers, including the Rhine River, Netherlands. For a five times increase in river flow (peak 11,900 m^3/s) over a two week period in the Rhine, the timescale of bedform growth was 17 h with a relaxation time of 140 days [*Wilbers and Ten Brinke*, 2003], which illustrates that the bedform adjustment time period can persist long after floods recess in big rivers.

[61] In general, streams with larger and/or longer lasting floods will be more likely to fully flush deeper and longer hyporheic flow paths. Simultaneous adjustments in velocity and bedform size during floods could have roughly offsetting effects on hyporheic fluxes. According to theory, the higher velocity of the flood should increase hyporheic flux whereas increasing wavelength of bedforms should reduce it [*Elliott and Brooks*, 1997]. Our field studies at Clear Run indicated that hyporheic fluxes increased during a flood by approximately an order of magnitude [*Bhaskar et al.*, 2012]. The bedform turnover flux also increased, driven by the taller and faster migrating bedforms, which further enhanced exchange of pore water in the shallow streambed (1.5 cm) by approximately a factor of five (Tables 2 and 5). Immediately after the flood the bedform turnover flux declined as larger bedforms became frozen in place. The hyporheic flux would also be expected to decline with the decrease in flow velocity. Actual adjustments in hyporheic flow are complicated by the growth of smaller bedforms on the back of storm-created ones, which maximizes streambed topographic variability, and which may enhance hyporheic flow as multiple scales become involved [*Stonedahl et al.*, 2010]. However, the deepest hyporheic flow paths (with relatively long residence times of tens of hours to days) only persist as long as it takes for larger bedforms to be cannibalized by smaller ones. At Clear Run these dynamics were compressed to just a few hours. Thus the flood-deepened hyporheic flow paths were not fully activated before larger bedforms were destroyed. As a result, bedform dynamics during the flood imposed limitations on expanding hyporheic flow. However, given the right circumstances of flood intensity and channel form (as shown through modeling by Martin and Jerolmack (submitted manuscript, 2012)), bedforms may require months or even years to be reworked back into the pre-flood pattern, and therefore could impose substantial controls on hyporheic flow over many spatial and temporal scales.

5.3.3. Fine Particulate Dynamics During the Flood

[62] Whereas the flood caused prolonged storage and delayed release of solute tracer, it caused the opposite effect (rapid entrainment) of the fine particulate tracer. A spike increase of two orders of magnitude in the fine particulate tracer concentration occurred immediately after the flood's arrival, at a time when only dilution was evident in the solute tracer (Figures 5 and 6). The tracer mass balance indicated that 30% of the fine particulates removed during base flow were entrained at the onset of the flood. Also, the newly entrained fine particulates did not redeposit immediately after the flood receded. An extended tail of elevated tracer concentration was observed (Figure 6b) that indicates the combined effects of storage-exchange, settling, hyporheic filtration, and entrainment over more than an hour as the bedforms readjusted into smaller features. Fine particulates are continually being transported in "jumps," i.e., due to release into the flow by entrainment and then deposition back to the bed. The variability in bedform size and migration rate introduces variability in waiting times between jumps. These processes are substantially modified by floods, when entrainment is maximized, but the basic processes occur at all times. Fine particle transport models that include all of these processes (bedform turnover, hyporheic flow and filtration of fines, and entrainment by floods) are rare.

5.4. Implications for Stream Ecology

[63] We used in-stream tracer experiments to investigate hydrologic and geomorphic controls on solute and organic matter transport processes and retention in streams. We build on previous studies, such as *Small et al.* [2008], who used paper to trace redistribution of CPOM in channels. Our research focused on hyporheic storage of solutes and FPOM and dynamics during floods. We found that FPOM accumulated beneath the depth of scour by small floods, which explains the measured peak in particulate organic carbon at 2–4 cm deep in the streambed, where organic carbon is 6 times higher compared to depths above or below. That finding suggests an important role for hyporheic retention of FPOM beneath migrating bedforms and scour caused by small floods, where it can potentially contribute to microbial respiration of organic carbon. *Valett et al.* [1994] found that after streams were swept clear by floods, the decomposition of buried particulate organic matter below the streambed was activated by hyporheic flow. Dissolved oxygen delivered with hyporheic flow enhances decomposition in flow paths that return to the stream with mineralized nutrients and also stimulates recovery of benthic periphyton. Those authors did not identify the mechanism of organic matter retention at

shallow depths below the level of flood scour. Our results suggest that advective transport and filtration of fine particulates in hyporheic flow paths is an important mode of FPOM storage that enhances recovery of periphyton communities and stream metabolism after floods. Ultimately, such processes have cascading influences on diversity and productivity of ecological communities at all trophic levels in streams [*Murdock et al.*, 2004].

6. Summary

[64] Our research highlights temporal dynamics of hyporheic flow and geomorphic processes and their effects on storage and retention of solutes and fine particles within streambed sediment. It is the first field study that we are aware of that simultaneously measured hyporheic flow and bedform dynamics and their differential effects on retention of both solute and fine particulates. We injected solute and fine particulate tracers together to partition the relative roles of hyporheic flow, bedform migration, and particle settling and filtration and how these processes changed during a flood.

[65] Solutes and fine particulates responded differentially to floods. Fine particulates were stored more shallowly in hyporheic flow paths, only two-thirds as deep as solutes, due to filtration, and thus fines were more easily mobilized by bedform migration. However, a significant proportion of fines penetrated deep enough (>1.5 cm) to be protected from entrainment by small floods and thus were retained much longer than solutes, until entrained by a flood that scours more deeply. Approximately 35% of fine particulates that were removed during base flow were transported deep enough before they were filtered and thus protected from entrainment during small floods. An equal proportion was rapidly entrained by a small flood from sites of deposition on the bed surface or the very shallow subsurface. In contrast, the flood drove solutes deeper into storage, up to 8 cm deep at base flow, and even deeper during the flood. Thus it is not surprising that fine particulates were efficiently mobilized whereas solutes were efficiently stored during a small flood. Although the higher stream velocities were short-lived during the passage of the flood, the larger bedforms persisted for hours after the flood recessed. Thus, three timescales defined dynamic bedform and hyporheic interactions. The relative timescales of flood duration, relaxation time of bedforms returning to pre-flood dimensions, and hyporheic residence times are all important. For short duration floods, the extended relaxation time of bedforms back to pre-flood dimensions can substantially prolong and increase the effects on hyporheic flow. In a small stream we found that even the extended relaxation time (several hours) was not enough to trigger substantial additional storage even though deeper hyporheic flow paths were hydraulically activated. The timescale of flushing the deeper hyporheic flow paths was tens of hours rather than hours. Higher magnitude floods and longer-lasting floods that typically occur in larger streams and rivers and are more likely to fully engage all of the flood-activated hyporheic flow paths.

[66] Our findings have important implications for retention and biological processing of organic matter and stream metabolism in sand-bed streams. In Clear Run only the fines that were advected deeper than the average bedform height during small floods were retained for significant time periods (tens of days to months, i.e., the approximate return period of intermediate to large floods). This zone is beneath the layer of active bedform turnover but has inputs of dissolved oxygen and dissolved and particulate organic carbon to fuel significant aerobic respiration and mineralization of nutrients in sand-bed streams where labile organic carbon may be limiting for many important biogeochemical reactions of interest (i.e., denitrification). Thus, bedform migration and growth and relaxation of bedforms during floods interact with hyporheic processes to influence key ecological processes in streams.

[67] **Acknowledgments.** This project was funded by NSF Grants EAR-0810140 and EAR-0814990 and the USGS HR&D and NAWQA Programs. We thank Eric Henry, Kim Duernberger, Matt Lettrich and Yvonne Marsan for assistance in the field and laboratory and we thank Trevor Langston for assistance with modeling. Any use of trade, firm, or product names is for descriptive purposes only and does not imply endorsement by the U.S. Government.

References

Allen, J. R. L. (1973), Phase differences between bed configuration and flow in natural environments, and their geological relevance, *Sedimentology*, *20*(2), 323–329, doi:10.1111/j.1365-3091.1973.tb02054.x.

Arnon, S., L. P. Marx, K. E. Searcy, and A. I. Packman (2010), Effects of overlying velocity, particle size, and biofilm growth on stream-subsurface exchange of particles, *Hydrol. Processes*, *24*(1), 108–114, doi:10.1002/hyp.7490.

Battin, T. J., L. A. Kaplan, J. D. Newbold, and C. M. E. Hansen (2003), Contributions of microbial biofilms to ecosystem processes in stream mesocosms, *Nature*, *426*(6965), 439–442, doi:10.1038/nature02152.

Battin, T. J., L. A. Kaplan, S. Findlay, C. S. Hopkinson, E. Marti, A. I. Packman, J. D. Newbold, and F. Sabater (2008), Biophysical controls on organic carbon fluxes in fluvial networks, *Nat. Geosci.*, *1*, 95–100, doi:10.1038/ngeo101.

Bhaskar, A. S., J. W. Harvey, and E. J. Henry (2012), Resolving hyporheic and groundwater components of streambed water flux using heat as a tracer, *Water Resour. Res.*, *48*, W08524, doi:10.1029/2011WR011784.

Boano, F., R. Revelli, and L. Ridolfi (2007), Bedform-induced hyporheic exchange with unsteady flows, *Adv. Water Resour.*, *30*(1), 148–156, doi:10.1016/j.advwatres.2006.03.004.

Briggs, M. A., M. N. Gooseff, C. D. Arp, and M. A. Baker (2009), A method for estimating surface transient storage parameters for streams with concurrent hyporheic storage, *Water Resour. Res.*, *45*, W00D27, doi:10.1029/2008WR006959.

Brigham, M. E., D. A. Wentz, G. R. Aiken, and D. P. Krabbenhof (2009), Mercury cycling in stream ecosystems. 1. Water column chemistry and transport, *Environ. Sci. Technol.*, *43*, 2720–2725.

Bukaveckas, P. A. (2007), Effects of channel restoration on water velocity, transient storage, and nutrient uptake in a channelized stream, *Environ. Sci. Technol.*, *41*(5), 1570–1576, doi:10.1021/es061618x.

Cardenas, M. B. (2008), Surface water-groundwater interface geomorphology leads to scaling of residence times, *Geophys. Res. Lett.*, *35*, L08402, doi:10.1029/2008GL033753.

Cardenas, M. B., and J. L. Wilson (2007), Dunes, turbulent eddies, and interfacial exchange with permeable sediments, *Water Resour. Res.*, *43*, W08412, doi:10.1029/2006WR005787.

Carling, P. A., E. Gölz, H. G. Orr, and A. Radecki-Pawlik (2000), The morphodynamics of fluvial sand dunes in the River Rhine near Mainz, Germany. I. Sedimentology and morphology, *Sedimentology*, *47*, 227–252, doi:10.1046/j.1365-3091.2000.00290.x.

Choi, J., J. W. Harvey, and M. H. Conklin (2000), Characterizing multiple timescales of stream and storage zone interaction that affect solute fate and transport in streams, *Water Resour. Res.*, *36*(6), 1511–1518, doi:10.1029/2000WR900051.

Cushing, C. E., G. W. Minshall, and J. D. Newbold (1993), Transport dynamics of fine particulate organic-matter in 2 Idaho streams, *Limnol. Oceanogr.*, *38*(6), 1101–1115, doi:10.4319/lo.1993.38.6.1101.

Dade, W. B., and P. F. Friend (1998), Grain size, sediment-transport regime and channel slope in alluvial rivers, *J. Geol.*, *106*, 661–676, doi:10.1086/516052.

Dietrich, W. E. (1982), Settling velocity of natural particles, *Water Resour. Res.*, *18*(6), 1615–1626, doi:10.1029/WR018i006p01615.

Duff, J. H., F. Murphy, C. C. Fuller, F. J. Triska, J. W. Harvey, and A. P. Jackman (1998), A mini drivepoint sampler for measuring pore water solute concentration in the hyporheic zone of sand-bottom streams, *Limnol. Oceanogr.*, *43*(6), 1378–1383, doi:10.4319/lo.1998.43.6.1378.

Einstein, H. A., and R. B. Krone (1962), Experiments to determine modes of cohesive sediment transport in salt water, *J. Geophys. Res.*, *67*(4), 1451–1461, doi:10.1029/JZ067i004p01451.

Elliott, A. H., and N. H. Brooks (1997), Transfer of nonsorbing solutes to a streambed with bed forms: Laboratory experiments, *Water Resour. Res.*, *33*(1), 137–151, doi:10.1029/96WR02783.

Gee, D. M. (1975), Bed form response to nonsteady flows, *J. Hydraul. Eng.*, *101*(3), 437–449.

Gerecht, K. E., M. B. Cardenas, A. J. Guswa, A. H. Sawyer, J. D. Nowinski, and T. E. Swanson (2011), Dynamics of hyporheic flow and heat transport across a bed-to-bank continuum in a large regulated river, *Water Resour. Res.*, *47*, W03524, doi:10.1029/2010WR009794.

Harvey, J. W., and C. F. Fuller (1998), Effect of enhanced manganese oxidation in the hyporheic zone on basin-scale geochemical mass balance, *Water Resour. Res.*, *34*(4), 623–636, doi:10.1029/97WR03606.

Harvey, J. W., and B. J. Wagner (2000), Quantifying hydrologic interactions between streams and their subsurface hyporheic zones, in *Streams and Ground Waters*, edited by J. A. Jones and P. J. Mulholland, pp. 3–44, Academic, San Diego, Calif., doi:10.1016/B978-012389845-6/50002-8.

Harvey, J. W., B. J. Wagner, and K. E. Bencala (1996), Evaluating the reliability of the stream tracer approach to characterize stream-subsurface water exchange, *Water Resour. Res.*, *32*(8), 2441–2451, doi:10.1029/96WR01268.

Harvey, J. W., J. E. Saiers, and J. T. Newlin (2005), Solute transport and storage mechanisms in wetlands of the Everglades, south Florida, *Water Resour. Res.*, *41*, W05009, doi:10.1029/2004WR003507.

Harvey, J. W., G. B. Noe, L. G. Larsen, D. J. Nowacki, and L. E. McPhillips (2011), Field flume reveals aquatic vegetation's role in sediment and particulate phosphorus transport in a shallow aquatic ecosystem, *Geomorphology*, *126*, 297–313, doi:10.1016/j.geomorph.2010.03.028.

Hünken, A., and M. Mutz (2007), Field studies on factors affecting very fine and ultra fine particulate organic matter deposition in low-gradient sand-bed streams, *Hydrol. Processes*, *21*(4), 525–533, doi:10.1002/hyp.6263.

Karwan, D. L., and J. E. Saiers (2009), Influences of seasonal flow regime on the fate and transport of fine particles and a dissolved solute in a New England stream, *Water Resour. Res.*, *45*, W11423, doi:10.1029/2009WR008077.

Karwan, D. L., and J. E. Saiers (2012), Hyporheic exchange and streambed filtration of suspended particles, *Water Resour. Res.*, *48*, W01519, doi:10.1029/2011WR011173.

Landon, M., et al. (2001), Comparison of instream methods for measuring hydraulic conductivity in sandy streambeds, *Ground Water*, *39*(6), 870–885, doi:10.1111/j.1745-6584.2001.tb02475.x.

Larsen, L. G., J. W. Harvey, and J. P. Crimaldi (2009), Morphologic and transport properties of natural organic floc, *Water Resour. Res.*, *45*, W01410, doi:10.1029/2008WR006990.

Lautz, L. K., and R. M. Fanelli (2008), Seasonal biogeochemical hotspots in the streambed around restoration structures, *Biogeochemistry*, *91*(1), 85–104, doi:10.1007/s10533-008-9235-2.

Minshall, G. W., S. A. Thomas, J. D. Newbold, M. T. Monaghan, and C. E. Cushing (2000), Physical factors influencing fine organic particle transport and deposition in streams, *J. N. Am. Benthol. Soc.*, *19*(1), 1–16, doi:10.2307/1468278.

Mulholland, P. J., et al. (2008), Stream denitrification across biomes and its response to anthropogenic nitrate loading, *Nature*, *452*(7184), 202–205, doi:10.1038/nature06686.

Murdock, J., D. Roelke, and F. Gelwick (2004), Interactions between flow, periphyton, and nutrients in a heavily impacted urban stream: Implications for stream restoration effectiveness, *Ecol. Eng.*, *22*(3), 197–207, doi:10.1016/j.ecoleng.2004.05.005.

Neilson, B. T., D. K. Stevens, S. C. Chapra, and C. Bandaragoda (2010), Two-zone transient storage modeling using temperature and solute data with multiobjective calibration: 2. Temperature and solute, *Water Resour. Res.*, *46*, W12521, doi:10.1029/2009WR008759.

Nelson, J. M., and J. D. Smith (1989), Evolution and stability of erodible channel beds, in *River Meandering*, *Water Resour. Monogr. Ser.*, vol. 12, edited by S. Ikeda and G. Parker, pp. 321–377, AGU, Washington, D. C., doi:10.1029/WM012p0321.

Newbold, J. D., S. A. Thomas, G. W. Minshall, C. E. Cushing, and T. Georgian (2005), Deposition, benthic residence, and resuspension of fine organic particles in a mountain stream, *Limnol. Oceanogr.*, *50*(5), 1571–1580, doi:10.4319/lo.2005.50.5.1571.

Nittrouer, J. A., M. A. Allison, and R. Campanella (2008), Bedform transport rates for the lowermost Mississippi River, *J. Geophys. Res.*, *113*, F03004, doi:10.1029/2007JF000795.

O'Connor, B. L., and J. W. Harvey (2008), Scaling hyporheic exchange and its influence on biogeochemical reactions in aquatic ecosystems, *Water Resour. Res.*, *44*, W12423, doi:10.1029/2008WR007160.

O'Connor, B. L., and M. Hondzo (2008), Enhancement and Inhibition of denitrification by fluid-flow and dissolved oxygen to stream sediment, *Environ. Sci. Technol.*, *42*, 119–125, doi:10.1021/es071173s.

O'Connor, B. L., M. Hondzo, and J. W. Harvey (2010), Predictive modeling of transient storage and nutrient uptake: Implications for stream restoration, *J. Hydraul. Eng.*, *136*(12), 1018–1032, doi:10.1061/(ASCE)HY.1943-7900.0000180.

O'Connor, B. L., J. W. Harvey, and L. E. McPhillips (2012), Thresholds of storm-induced bed disturbances and their effects on stream metabolism in an agricultural river. *Water Resour. Res.*, *48*, W08504, doi:10.1029/2011WR011488.

Packman, A. I., and N. H. Brooks (2001), Hyporheic exchange of solutes and colloids with moving bed forms, *Water Resour. Res.*, *37*(10), 2591–2605, doi:10.1029/2001WR000477.

Packman, A. I., and J. S. MacKay (2003), Interplay of stream-subsurface exchange, clay particle deposition, and streambed evolution, *Water Resour. Res.*, *39*(4), 1097, doi:10.1029/2002WR001432.

Packman, A. I., N. H. Brooks, and J. J. Morgan (2000), Kaolinite exchange between a stream and streambed: Laboratory experiments and validation of a colloid transport model, *Water Resour. Res.*, *36*(8), 2363–2372, doi:10.1029/2000WR900058.

Palmer, M. R., H. M. Nepf, T. J. R. Petterson, and J. D. Ackerman (2004), Observations of particle capture on a cylindrical collector: Implications for particle removal in aquatic ecosystems, *Limnol. Oceanogr.*, *49*(1), 76–85, doi:10.4319/lo.2004.49.1.0076.

Paul, M. J., and R. O. Hall (2002), Particle transport and transient storage along a stream-size gradient in the Hubbard Brook Experimental Forest, *J. N. Am. Benthol. Soc.*, *21*(2), 195–205, doi:10.2307/1468409.

Rehg, K. J., A. I. Packman, and J. Ren (2005), Effects of suspended sediment characteristics and bed sediment transport on streambed clogging, *Hydrol. Processes*, *19*, 413–427, doi:10.1002/hyp.5540.

Reynolds, W. D., D. E. Elrick, E. G. Youngs, A. Amoozegar, and H. W. G. Booltink (2002), Ring or cylinder infiltrometers, in *Methods of Soil Analysis: Part 4—Physical Methods*, edited by J. H. Dane and G. C. Topp, pp. XX–XX, Soil Sci. Soc. of Am., Madison, Wis.

Runkel, R. L. (1998), One-Dimensional Transport with Inflow and Storage (OTIS): A solute transport model for streams and rivers, *U.S. Geol. Surv. Water Resour. Invest. Rep.*, *98–4018*, 73 p.

Saiers, J. E., J. W. Harvey, and S. E. Mylon (2003), Surface-water transport of suspended matter through wetland vegetation of the Florida Everglades, *Geophys. Res. Lett.*, *30*(19), 1987, doi:10.1029/2003GL018132.

Searcy, K. E., A. I. Packman, E. R. Atwill, and T. Harter (2006), Deposition of *Cryptosporidium* oocysts in streambeds, *Appl. Environ. Microbiol.*, *72*(3), 1810–1816.

Small, M. J., M. W. Doyle, R. L. Fuller, and R. B. Manners (2008), Hydrologic versus geomorphic limitation on CPOM storage in stream ecosystems, *Freshwater Biol.*, *53*, 1618–1631, doi:10.1111/j.1365-2427.2008.01999.x.

Stonedahl, S. H., J. W. Harvey, A. Wörman, M. Salehin, and A. I. Packman (2010), A multiscale model for integrating hyporheic exchange from ripples to meanders, *Water Resour. Res.*, *46*, W12539, doi:10.1029/2009WR008865.

Thibodeaux, L. J., and J. D. Boyle (1987), Bedform-generated convective-transport in bottom sediment, *Nature*, *325*(6102), 341–343, doi:10.1038/325341a0.

Thomas, S. A., J. D. Newbold, M. T. Monaghan, G. W. Minshall, T. Georgian, and C. E. Cushing (2001), The influence of particle size on seston deposition in streams, *Limnol. Oceanogr.*, *46*(6), 1415–1424, doi:10.4319/lo.2001.46.6.1415.

Tipping, E., C. Woof, and K. Clarke (1993), Deposition and resuspension of fine particles in a riverine dead zone, *Hydrol. Processes*, *7*(3), 263–277, doi:10.1002/hyp.3360070304.

Triska, F. J., V. C. Kennedy, R. J. Avanzino, G. W. Zellweger, and K. E. Bencala (1989), Retention and transport of nutrients in a third-order stream in northwestern California: Hyporheic processes, *Ecology*, *70*(6), 1893–1905, doi:10.2307/1938120.

Valett, H. M., S. G. Fisher, N. B. Grimm, and P. Camill (1994), Vertical hydrologic exchange and ecological stability of a desert stream ecosystem, *Ecology*, *75*(2), 548–560, doi:10.2307/1939557.

Wagner, B. J., and J. W. Harvey (1997), Experimental design for estimating parameters of rate-limited mass transfer: Analysis of stream tracer studies, *Water Resour. Res.*, *33*(7), 1731–1741.

Webster, J. R., E. F. Benfield, S. W. Golladay, B. H. Hill, L. E. Hornick, R. F. Kazmierczak, and W. B. Perry (1987), Experimental studies of physical factors affecting seston transport in streams, *Limnol. Oceanogr.*, *32*(4), 848–863, doi:10.4319/lo.1987.32.4.0848.

Wilbers, A. W. E., and W. B. M. Ten Brinke (2003), The response of subaqueous dunes to floods in sand and gravel bed reaches of the Dutch Rhine, *Sedimentology*, *50*(6), 1013–1034, doi:10.1046/j.1365-3091.2003.00585.x.

Wondzell, S. M., and F. J. Swanson (1996), Seasonal and storm dynamics of the hyporheic zone of a 4th-order mountain stream. 1. Hydrologic processes, *J. N. Am. Benthol. Soc.*, *15*(1), 3–19, doi:10.2307/1467429.